Geochemistry, Geophysics, Geosystems®

RESEARCH ARTICLE
10.1029/2023GC010866

Key Points:

- New Zealand's Neogene explosive volcanism based on the marine tephra record
- Geochemical fingerprinting of marine tephra layers across the study area to establish volcanic events
- Insights into geochemical variations with time, repose times and spatiotemporal distribution

Supporting Information:

Supporting Information may be found in the online version of this article.

Correspondence to:

K. Pank,
kpank@geomar.de

Citation:

Pank, K., Kutterolf, S., Hopkins, J. L., Wang, K.-L., Lee, H.-Y., & Schmitt, A. K. (2023). Advances in New Zealand's tephrochronostratigraphy using marine drill sites: The Neogene. *Geochemistry, Geophysics, Geosystems*, *24*, e2023GC010866. https://doi.org/10.1029/2023GC010866

Received 18 JAN 2023
Accepted 2 JUN 2023

Author Contributions:

Conceptualization: S. Kutterolf, J. L. Hopkins
Data curation: K. Pank, K.-L. Wang, H.-Y. Lee, A. K. Schmitt
Funding acquisition: S. Kutterolf, J. L. Hopkins
Investigation: K. Pank, S. Kutterolf
Methodology: S. Kutterolf, J. L. Hopkins
Project Administration: S. Kutterolf
Supervision: S. Kutterolf, J. L. Hopkins
Visualization: K. Pank
Writing – original draft: K. Pank

Advances in New Zealand's Tephrochronostratigraphy Using Marine Drill Sites: The Neogene

K. Pank[1], S. Kutterolf[1], J. L. Hopkins[2], K.-L. Wang[3,4], H.-Y. Lee[3], and A. K. Schmitt[5,6]

[1]GEOMAR Helmholtz Centre for Ocean Research Kiel, Kiel, Germany, [2]School of Geography Environment and Earth Science, Victoria University of Wellington, Wellington, New Zealand, [3]Institute of Earth Sciences, Academia Sinica, Taipei, Taiwan, [4]Department of Geosciences, National Taiwan University, Taipei, Taiwan, [5]John de Laeter Centre, Curtin University, Perth, WA, Australia, [6]Institut für Geowissenschaften, Universität Heidelberg, Heidelberg, Germany

Abstract Three volcanic arcs have been the source of New Zealand's volcanic activity since the Neogene: Northland arc, Coromandel Volcanic Zone (CVZ) and Taupō Volcanic Zone (TVZ). The eruption chronology for the Quaternary, sourced by the TVZ, is well studied and established, whereas the volcanic evolution of the precursor arc systems, like the CVZ (central activity c. 18 to 2 Ma), is poorly known due to limited accessibility to, or identification of, onshore volcanic deposits and their sources. Here, we investigate the marine tephra record of the Neogene, mostly sourced by the CVZ, of cores from IODP Exp. 375 (Sites U1520 and U1526), ODP Leg 181 (Sites 1123, 1124 and 1125), IODP Leg 329 (Site U1371) and DSDP Leg 90 (Site 594) offshore of New Zealand. In total, we identify 306 primary tephra layers in the marine sediments. Multi-approach age models (e.g. biostratigraphy, zircon ages) are used in combination with geochemical fingerprinting (major and trace element compositions) and the stratigraphic context of each marine tephra layer to establish 168 tie-lines between marine tephra layers from different holes and sites. Following this approach, we identify 208 explosive volcanic events in the Neogene between c. 17.5 and 2.6 Ma. This is the first comprehensive study of New Zealand's Neogene explosive volcanism established from tephrochronostratigraphic studies, which reveals continuous volcanic activity between c. 12 and 2.6 Ma with an abrupt compositional change at c. 4.5 Ma, potentially associated with the transition from CVZ to TVZ.

Plain Language Summary Since 18 Ma, volcanic activity in New Zealand is dominantly sourced by the Coromandel Volcanic Zone (CVZ). Most caldera systems of the CVZ identified so far are located on Coromandel Peninsula in the NW of North Island, New Zealand, but studies of the CVZ are rare mainly due to the limited accessibility of its volcanic deposits, as well as missing stratigraphic continuity between different outcrops and the volcanic source. Here, our ocean drilling tephra record—mainly volcanic ash from explosive eruptions, distributed and falling out over the ocean—has a great potential to reveal the eruption history of the CVZ because it is preserved in marine sediments in a nearly undisturbed stratigraphic context. We analyzed ∼400 marine tephra layers from multiple ocean sediment cores off the coast of New Zealand for their geochemical glass compositions and identified 306 as largely undisturbed ash deposits. These primary ash deposits correspond to a total number of 208 Neogene volcanic events. Different dating methods result in a continuous marine tephra record for the last 12 Ma, equivalent to a unique and most complete eruptive history for the CVZ. This enables us to further unravel changes in the composition of the associated magmas with time.

1. Introduction

Volcanic arc systems along plate boundaries are persistent systems that can exist in a relatively steady state over millions of years (e.g. active margin of South America; Booden et al., 2012). However, if subduction parameters change, the associated arc volcanism can also change in space and time, ultimately affecting the geochemical and eruptive character of the corresponding magmatism. The plate boundary between the Pacific and Australian Plates in the southwestern Pacific is an example of an unstable convergent plate boundary with associated evolving arc systems since the Late Cenozoic (Booden et al., 2012) and New Zealand has been under the influence of the re-adjusting plate boundaries between the Pacific and Australian plates for the last 40 Myr years. Since 25 Ma years, these tectonic changes are documented by evolving arc volcanism. The earliest subduction-related volcanic activity on the Zealandia continent was probably located along the Northland arc (Northland Peninsula, Figure 1a) with relatively silica-poor volcanism producing mainly basalts and andesites (Smith et al., 1989). Over time, the geochemical composition of the arc shifted toward andesitic

Writing – review & editing: K. Pank, S. Kutterolf, J. L. Hopkins, K.-L. Wang, H.-Y. Lee, A. K. Schmitt

and rhyolitic volcanism in the Coromandel Volcanic Zone (CVZ; Skinner, 1986), and finally to highly silicic volcanism in the Taupō Volcanic Zone (TVZ; Figure 1), which still represents the zone of active volcanism in New Zealand today (Booden et al., 2012; King, 2000; Wilson et al., 1995). The TVZ is considered one of the most frequently active rhyolitic systems worldwide, having produced many caldera-forming eruptions from several prominent volcanic centers over the last 2 million years (e.g. Allan et al., 2008; Houghton et al., 1995; Pittari et al., 2021). In order to understand the full volcanic potential of the TVZ, estimate possible future shifts in geochemistry and thus explosive character of this volcanic arc, it is important to study the evolution of its precursory activity. Studies about the volcanic evolution of the Northland arc and volcanism at the Neogene CVZ are limited mostly due to the restricted subaerial accessibility of volcanic deposits and source volcanoes, or even their identification because of geomorphological, tectonic, and hydrothermal modifications over millions of years. However, the overall interest in the geochemical evolution of precursory arcs is rising and recent studies (e.g. Booden et al., 2012; Pittari et al., 2021) present detailed insights into the spatiotemporal evolution of CVZ volcanism. In order to study the long-term evolution of the CVZ and possible geochemical differences between the Quaternary and Neogene volcanic arcs, the establishment of a comprehensive eruptive history is required. Examples from other arc systems (e.g. Hellenic arc, Central American Volcanic Arc; e.g. Kutterolf et al., 2021a; Schindlbeck, Kutterolf, Freundt, Straub, et al., 2016) have shown that nonerosive marine environments provide the most complete eruptive record of volcanic zones by preserving widely distributed volcanic ash (Carey, 2000; Carey & Sigurdsson, 2000; Keller et al., 1978; Kutterolf, Freundt, Peréz, et al., 2008, Kutterolf, Freundt, & Peréz, 2008; Ledbetter, 1985; Schindlbeck, Kutterolf, Freundt, Alvarado, et al., 2016; Schindlbeck, Kutterolf, Freundt, Straub, et al., 2016; Schindlbeck, Kutterolf, et al., 2018). Marine sediments can even conserve small eruptions which might not be preserved in the onshore sedimentary record, allowing the establishment of the most complete eruptive histories of volcanic regions found within these distal marine locations (Freundt et al., 2022).

In this study, we present new marine tephra layers from IODP Expedition 375 (proximal marine tephra record), and we revisit marine tephra layers from ODP Leg 181, IODP Leg 329 and DSDP Leg 90 (distal marine tephra record). The proximal and distal submarine tephra records are connected and integrated, allowing us to establish the most complete tephrochronostratigraphy of New Zealand's Neogene explosive volcanism.

2. Geological Setting

Neogene (23–2.6 Ma) volcanic-arc related edifices and volcanic deposits are found on the northwesternmost tips of the North Island, New Zealand; more specifically on Northland Peninsula and on Coromandel Peninsula, two parallel peninsulas associated with continental arc systems (Figure 1a; e.g. Adams et al., 1994; Booden et al., 2012; Briggs et al., 2005; Hayward et al., 2001; Herzer, 1995). On Northland Peninsula basalt- and andesite-dominated shield and cone volcanism with limited silicic activity were identified as products of the Northland volcanic arc (Smith et al., 1989). The onset of volcanic activity along the Northland arc is dated to c. 23.5 Ma (Hayward et al., 2001). From c. 18 Ma, while volcanic activity along the Northland arc decreased, the Coromandel Volcanic Zone (CVZ) became active and produced more evolved andesite-to rhyolite-dominated volcanism (Skinner, 1986). Most subaerially identified volcanic deposits and edifice structures of the CVZ are located on Coromandel Peninsula. The Coromandel Peninsula is located at the continental tip of the extinct Colville Ridge, which trends NNE and was active as early as c. 17 Ma. This coeval arc volcanism led to the interpretation of a single NNE-trending Miocene volcanic arc with a total length of ∼2,500 km (Herzer, 1995). From c. 12 Ma on, volcanism of the CVZ migrated over time from the NNW toward the SSE and ultimately to the central North Island (Figure 1b). Simultaneously the geochemistry of volcanism shifted from initially andesitic compositions to mixed basaltic, andesitic and rhyolitic compositions (Booden et al., 2012). These changes in geochemical compositions are most likely due to variations in the tectonic setting, for example, during phases of extension silica-rich volcanism is likely to occur (Booden et al., 2012). Since 3 Ma, the spatiotemporal evolution of North Island volcanism reflects a south-eastward migration of the volcanic arc toward its present position on the central North Island along the TVZ. The temporal transition of volcanic activity from CVZ to TVZ is assigned to the onset of andesitic calc-alkaline volcanism, roughly dated to between 4 and 2 Ma (Carter et al., 2003; Houghton et al., 1995; Stipp, 1968; Wilson et al., 1995; Wilson & Rowland, 2016), and the first volcanic activity attributed to the TVZ occurred at c. 2 Ma at Mangakino Volcanic Centre (MVC, Figure 1b) with increased silica-rich volcanism.

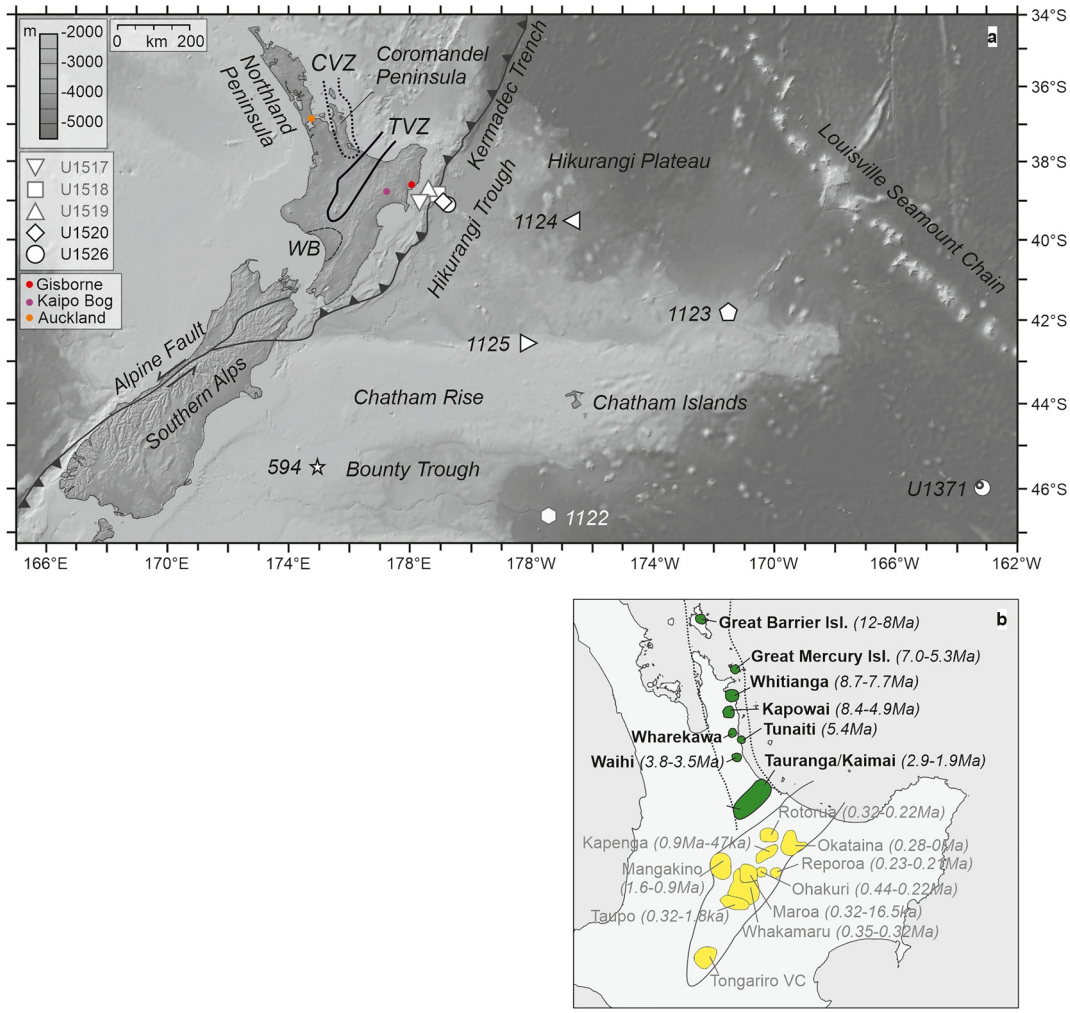

Figure 1. (a) Overview map of New Zealand including simplified plate boundaries. Neogene sediments with intercalated tephra layers were recovered from Sites U1520 and U1526 (IODP Exp. 375), Sites 1123, 1124 and 1125 (ODP Leg 181), Site 594 (DSDP Leg 90) and Site U1371 (IODP Leg 329). CVZ: Coromandel Volcanic Zone, TVZ: Taupō Volcanic Zone, WB: Whanganui Basin. Map created with GeoMapApp, GMRT (Ryan et al., 2009). B) Identified volcanic centers of the Neogene CVZ (green signature) and Quaternary TVZ (yellow signature) after Briggs et al. (2005), Hopkins and Seward (2019) and Pittari et al. (2021).

2.1. Evolution of the CVZ

Earliest descriptions of volcanic deposits on North Island, New Zealand, are attributed to the discovery of gold in the mid to late nineteenth century and exploration of mineralized volcanic zones at Coromandel Peninsula. For example, Skinner (1976, 1986, 1993) regionally mapped and characterized volcanic deposits, but stratigraphic work concentrating on deposits and geochemistry was established more recently, mostly by Adams et al. (1994), Briggs et al. (2005) and Booden et al. (2012). The volcanism evolved through time, erupting a range of calc-alkaline basaltic andesites, andesites and dacites. At c. 12 Ma the first rhyolitic eruptions have been identified, however there remains evidence of basaltic through to dacitic eruptions throughout the life-time of the CVZ (e.g., Adams et al., 1994; Booden et al., 2012; Skinner, 1986). Volcanism in the CVZ is thought to have initiated close to Great Barrier Island (Figure 1b) as basaltic (Mercury basalts) and andesitic rocks at c. 18 Ma, with Booden et al. (2012) concluding that volcanism in the CVZ occurred continuously until the inception of the TVZ. The authors state that the basalts and andesites of the early and later series of the CVZ are geochemically and isotopically comparable, likely indicating related magmatic processes or similar sources for the c. 16 Ma eruptive life-time of the CVZ.

Several silicic volcanic centers or calderas are currently recognized in the CVZ, which have evolved in a southward progression through time: Great Barrier Island (c. 12–8 Ma), Great Mercury Island (c. 7–5.3 Ma), Whitianga

(c. 8.7–7.7 Ma), Kapowai (c. 8.4–4.9 Ma), Wharekawa (not dated), Tunaiti (c. 5.4 Ma), Waihi (c. 4.5–3.0 Ma), Tauranga and Kaimai (Omanawa caldera, c. 2.9–1.9 Ma) (Figure 1b; Booden et al., 2012; Briggs et al., 2005; Hopkins & Seward, 2019; Pittari et al., 2021).

Studies about specific caldera systems of the CVZ are rare, however, the youngest two volcanic systems have more in depth studies published: (a) Waihi caldera (Figure 1b) dated as 4.5–3.0 Ma (Briggs et al., 2005), and 4.5–3.5 Ma (Julian, 2016) has been shown to have two eruptive episodes with associated ignimbrite deposits; Owharoa (c. 3.8 Ma) and Waikino (c. 3.5 Ma) (Brathwaite & Christie, 1996; Julian, 2016), and (b) Tauranga Volcanic Centre (TgaVC; Figure 1b) dated as c. 2.7–1.9 Ma (Briggs et al., 2005), and 2.95–1.9 Ma (Pittari et al., 2021 and references therein) consisted of andesitic to rhyolitic volcanism from two previously recognised volcanic centers (Tauranga and Kaimai, Figure 1b), with several ignimbrite-forming eruptions toward its end that may be related to the Omanawa caldera (Pittari et al., 2021 and references therein). The spatiotemporal transition of volcanic activity located at the CVZ to TVZ is still under debate, but Pittari et al. (2021) identified volcanic deposits of potentially contemporaneous volcanic activity from the TgaVC (CVZ) and Mangakino Volcanic Centre (TVZ; Figure 1b).

2.2. Dispersal of Volcanic Material

Explosive arc volcanism is usually associated with large eruptions that widely disperse volcanic material, such as tephra, lahars and pyroclastic flows across land and oceans 10s to 1,000s kilometres from source (e.g. Freundt et al., 2022 and references therein).

In New Zealand, westerly to south-westerly stratospheric winds transport tephra far offshore into the Pacific Ocean where the tephra is preserved in the marine sediments off the east coast (e.g. Allan et al., 2008; Carter et al., 2004). Additionally, rivers and re-entrants towards the open ocean cause a high terrigenous sedimentary input into the Pacific also transporting potentially reworked volcanic material from onland (Pouderoux et al., 2012). However, so far these studies (e.g. Pouderoux et al., 2012) mostly focus on the Quaternary tephra dispersal. During the Neogene, the dispersal of tephra might have been different to what is known for the Quaternary, for example, due to the influence of paleowinds and/or plate tectonics, but studies about regional-specific paleoclimate including wind directions for New Zealand are rare and mostly focus on glacial and interglacial cycles, or are poorly resolved in terms of local effects (e.g. Pole, 2003; Rea and Bloomstine, 1986). A comparison of tephra occurrence in drill sites from ODP Leg 181 (Figure 1a) and DSDP Leg 90 (Site 594 in Figure 1a, and Sites 592 and 593 west of New Zealand, not shown) shows the overall predominating westerly winds in New Zealand, leading to numerous macroscopic tephra layers in sediments from ODP Leg 181 and only very few macroscopic tephra layers in Sites 592 and 593 (Carter et al., 2004; Gardner et al., 1986; Nelson et al., 1986). Moreover, the arrangement of ODP Leg 181 drill sites provides insights into regional changes of paleowinds over the last 12 million years due to the occurrence or absence of tephras in the marine sediments of Sites 1123, 1124 and 1125. For example, between 11 and 9 Ma most tephras are present in Site 1125 (Figure 1a), whereas tephras are rare in Site 1124 or absent in Site 1123, indicating predominant winds toward the southeast (Carter et al., 2004). From 9 Ma on, most tephras are present in drill sites to the east (Sites 1123 and 1124), explained by increasing westerly winds, whereas from 7 Ma on intensified dispersal of tephra toward the south is observed (Carter et al., 2004).

Even though there seem to be shifts of tephra occurrence in the drill sites over time, the ODP Leg 181 sites were located further offshore from the volcanic source due to plate rearrangements until at least 4 Ma ago, generally limiting the ability of fallout tephra and pyroclastic flows to reach the depositional environment (see Section 7.2; Carter et al., 2004; King, 2000; Strogen et al., 2022).

3. Previous Neogene Tephra Studies

3.1. Onshore Tephrostratigraphy

New Zealand has been in the focus of numerous tephra studies for >100 years, pioneered for example by Froggatt (1983) and Lowe (1990) who established the first approach for the geochemical fingerprinting of individual tephra layers of New Zealand's Quaternary volcanism using electron-probe microanalysis (EMP). Several detailed studies led to a precise reconstruction of the volcanic record of the last 61 ka (e.g. Hopkins,

Bidmead, et al., 2021). Older Quaternary TVZ deposits and especially those older than the Whakamaru group ignimbrites (c. 0.35 Ma; Whakamaru Volcanic Centre; Figure 1b) are poorly constrained due to the fragmentary terrestrial record of volcanic deposits and the limited stratigraphic control of terrestrial deposits with unknown ages (Allan et al., 2008; Hopkins, Lowe, et al., 2021; Shane, 2000; Wilson et al., 1995). Moreover, the data of most studies are sparsely or not at all published, and often limited to major element compositions, hindering present studies to access and use the data. Studies with a specific focus on the Neogene volcanic history of New Zealand are even more rare and neither systematic, nor truly comprehensive as discussed in Hopkins and Seward (2019). However, in recent years more volcanological studies have been undertaken (e.g. Booden et al., 2012; Briggs et al., 2005; Hopkins & Seward, 2019; Julian, 2016; Pittari et al., 2021), improving the knowledge of volcanic onshore deposits, and therefore further facilitating the use of existing data for distant correlation purposes.

Entire tephra successions and cycles of volcanic activity can be investigated on North Island, New Zealand, because uninterrupted, marine sediment intervals were uplifted, e.g. in the Whanganui Basin and at Mahia Peninsula (Figure 1a). The Whanganui Basin contains a stratigraphic record of marine sediments with several intercalated tephra beds from c. 0.5–3.1 Ma (Grant et al., 2018; Naish et al., 1996; Pillans et al., 2005; Sefton, 2015), and Mahia Peninsula contains an up-lifted sequence of tephra deposits within marine sediments from c. 7 to 9 Ma (Shane et al., 1998). In addition, Hopkins and Seward (2019) sampled late Miocene to Pleistocene marine sediments from several terrestrial locations around Hawke's Bay (Figure 1a, large bay of the eastern North Island), and acquired a comprehensive Neogene terrestrial tephra data set including major and trace element compositions of volcanic deposits, and where possible direct ages of individual tephra beds (c. 1.6–7.0 Ma).

3.2. Previous Marine Tephra Studies

Marine tephra studies have focused on tephra layers within marine sediments from ODP Leg 181 (~700–1,100 km offshore; Figure 1a) covering the Quaternary (e.g., Allan et al., 2008; Alloway et al., 2005) and part of the Neogene (Carter et al., 2003, 2004; Stevens, 2010). Carter et al. (2003, 2004) established a c. 12 Myr long record for ODP Leg 181 Sites and analyzed discrete tephra beds greater than 1 cm for their major element compositions and used combined paleomagnetic records, biostratigraphic datums and an orbitally tuned, benthic $\delta^{18}O$ record to obtain age models for the tephra record at Sites 1122, 1123 and 1124. These are assisted by direct age dating from glass isothermal plateau fission track ages from tephras of Site 1124. Site 1125 has a less-well constrained age model but the well-established biostratigraphic markers and paleomagnetic records of Sites 1123 and 1124, partly found in Site 1125 as well, enable an adaption of the age model for Site 1125 (Carter et al., 2004). Site 1125 records the oldest phase of increased CVZ volcanic activity between c. 10.6 to 10 Ma (Adams et al., 1994; Carter et al., 2004). The sediment record of Site 1123 is considered uninterrupted to 15 Ma and reliable to 20 Ma, except for two hiatuses each <100 Kyr. The record of Site 1124 is continuous to 11 Ma and reliable to 27 Ma, except for three mid-late Miocene hiatuses of 1.5–5.0 Myr duration (Carter et al., 2004). The most regular volcanic activity throughout the last c. 12 Ma is recorded at Site 1124, probably due to its proximity to the volcanic source area (Carter et al., 2004).

Stevens (2010) re-visited cores from Site 1124, sampled discrete tephra layers, and conducted major and trace element analyses which partly overlap between c. 2.1 Ma and c. 8.4 Ma with the ones studied by Carter et al. (2004). Periods of volcanic quiescence during the Miocene continued for c. 0.8 Myr, whereas non-tephra deposition during the Pliocene (late Neogene) was only <0.5 Myr (Stevens, 2010). Based on the number of eruptive events in Site 1124, Stevens (2010) calculated eruption frequencies of one eruption per 99 Kyr for the late Miocene and one per 74 Kyr for the Pliocene; however, Shane et al. (1998) suggest that the records of both depositional environments, terrestrial and marine, probably underestimate the volcanic activity of the CVZ.

4. Methods

4.1. Deep Sea Drilling Cores

During IODP Expedition 375, five proximal deep-sea sites (Sites U1517, U1518, U1519, U1520 and U1526) were drilled along a transect across the Hikurangi subduction margin ~40–100 km offshore of the North Island of New Zealand (Figure 1a). For this study, the drill sites U1520 (holes C and D), located in the Hikurangi Trough, and U1526 (hole A), located on Tūranganui Knoll, are relevant. Sampling of discrete tephra layers occurred during the expedition. The proximal sediment record of IODP Exp. 375 is complemented by the distal deep-sea

drill sites 1122, 1123, 1124 and 1125 from ODP Leg 181 located on the Hikurangi Plateau ~700 - 1,100 km offshore to the south and southeast of the IODP Exp. 375 drill sites (Figure 1a). Tephras of Neogene age were identified mostly based on shipboard data and previous studies (e.g., Allan et al., 2008; Alloway et al., 2005; Carter et al., 2004) in Sites 1123, 1124 and 1125, and sampled at the IODP Gulf Coast Repository at Texas A&M University, College Station, Texas. Additionally, Neogene age deposits from cores from Sites 594 (DSDP Leg 90) and U1371 (IODP Leg 329) were resampled at the Gulf Coast Repository.

Our Neogene data set includes ~400 ash-rich samples. The complete data set (Quaternary and Neogene) including a detailed description of recovered sediments from individual drill sites, methods, and geochemical compositions is published in a data report by Pank et al. (2023).

4.2. Sample Preparation

All marine tephra samples were disaggregated in an ultrasonic bath and, where applicable, carefully crushed with a mortar, and then wet-sieved with deionized water into the grain size fractions 63–125 μm, >125 μm and where necessary 32–63 μm. The samples were subsequently dried at ~50°C for at least 12 hr.

For the compositional analysis of the samples by electron probe microanalysis (EPMA) and laser ablation-inductively coupled plasma-mass spectrometry (LA-ICP-MS) the 63–125 μm fraction of each sample is embedded with epoxy resin in a predrilled hole on an acrylic tablet (twelve samples per mount). The mounts are ground on sandpaper (four grit sizes) for two minutes each in order to remove excess resin, bubbles or scratches on the sample's surfaces. Subsequently and in order to ensure a smooth surface of each sample, the mounts were polished on a TegraPol-31 (Struers) using three diamond suspensions (9, 3 and 1 μm) and corresponding polishing discs for 4 min each. The mounts were carbon-coated before analysis with the electron microprobe to ensure proper electron flow.

4.3. Analytical Techniques

4.3.1. Electron Microprobe (EMP) and Data Reduction

Individual glass shard analyses, ~7,500 analyses in total, for major and minor (Na_2O, K_2O, FeO, SiO_2, Al_2O_3, CaO, TiO_2, MgO, MnO, P_2O_5) elements were conducted on epoxy embedded samples using a JEOL JXA 8200 wavelength dispersive electron microprobe (EMP) at GEOMAR Helmholtz Centre for Ocean Research Kiel (Germany) adopting the methods from Kutterolf et al. (2011). For every 80 individual glass shard analyses the standard materials Lipari Obsidian (rhyolite; Hunt and Hill, 2001) and VGA-99 (basalt from Makaopuhi Lava Lake; Jarosewich et al. (1980) and Jarosewich (2002)) were repeatedly analyzed (two measurements per standard) to monitor the accuracy of measurements. The resulting standard deviations over the entire measurement period are <6% for all oxides except for MnO (Tables S3 and S4 in Supporting Information S2). Per sample, if possible, 20 individual glass shards were analyzed and the compositions were averaged in order to geochemically characterize each individual tephra layer. In rare cases, for example if the sample was too altered, less than 20 glass shards were selected for analyses. Analyses with total oxides less than 90 wt% were excluded from the data set to avoid effects of alteration. However, exceptions were made for some tephra layers in Site U1520C where data acquisition was comparably difficult and some analyses resulted in totals <90 wt%. Accidentaly measured microcrystals and glass shards with exotic compositions, compared to the average composition of the tephra layer, were excluded. All analyses were normalized to 100 wt% to eliminate possible effects of post-depositional hydration and minor deviations in the focus of the electron beam.

In total ~6,900 individual analyses passed the quality check as described above. Publication relevant geochemical data are given in Tables S1, and S7–S13 in Supporting Information S2.

4.3.2. Laser Ablation-Inductively Coupled-Mass Spectrometry (LA-ICP-MS) and Data Reduction

For each sample five glass shards were selected for trace element analysis. These glass shards were previously measured on the EMP in order to obtain their individual calcium and silica concentrations, which are used as internal standards to calibrate each trace element analysis. The trace element compositions were analyzed on a Photon Machines Analyte G2 (193 nm) excimer laser ablation system linked to a high-resolution ICP-MS (Agilent 7900) at the Institute of Earth Sciences, Academia Sinica in Taipei (Taiwan) using the methods described in

Kutterolf et al. (2021a). Data reduction was performed using GLITTER © software immediately following each ablation analysis (van Achterberg et al., 2001). The international glass standard BCR-2G (Jochum et al., 2005) was analyzed every ten individual measurements in order to monitor the accuracy. The repeated analyses of the standard material assured the correction of matrix effects and signal drift of the LA-ICP-MS, just as it monitors the differences of the ablation efficiency between sample and reference material (Günther et al., 1999). The reference material NIST SRM612 was used for external calibration, with reference data taken from Norman et al. (1996) (Table S5 in Supporting Information S2). The limits of detection (LOD) for most trace elements is <100 ppb, for rare earth elements (REE) the LOD is around 10 ppb. The analytical precision compared to the international glass standard BCR-2G is generally better than 10% (except for Ta) over the entire measurement period (Table S6 in Supporting Information S2).

We analyzed ∼170 Neogene samples for their trace element compositions, resulting in ∼780 individual analyses. All data are reported in Tables S1, and S7–S13 in Supporting Information S2.

4.4. U-Pb Zircon Geochronology

U-Pb zircon ages were collected for selected tephra layers at Heidelberg University, Germany (Table S2 in Supporting Information S2). Zircon crystals were embedded in epoxy, sectioned using SiC and diamond abrasives, and then imaged using a Gatan MiniCL cathodoluminescence detector (LEO 440 scanning electron microscope). Zircon U-Pb dating was conducted on a CAMECA IMS 1280-HR secondary ion mass spectrometer (SIMS) with a ∼20 nA primary beam focused to a ∼40 µm diameter spot. The zircon reference Temora 2 (417 Ma; Black et al., 2004) was used to calibrate relative sensitivities of U and Pb and after correction for common Pb using measured ^{207}Pb with a zero-age model Pb composition of ^{207}Pb/^{206}Pb = 0.836 (Stacey and Kramers, 1975), individual ^{206}Pb/^{238}U ages were calculated. The ages were adjusted for initial disequilibrium with correction factors D_{230} = 0.2 and D_{231} = 3. Abundances for U and Th were estimated from measured ^{238}U/$^{94}Zr_2O$ and Th/U with relative sensitivities of 0.00689 and 0.690 determined on reference zircon 91500 and Temora 2, respectively. Replicate analyses of reference zircon 91500 were performed to assure accuracy and obtained an average of 1,064 ± 8 Ma (n = 3), in close agreement with the reported age of 1,065 Ma (Wiedenbeck et al., 1995).

4.5. Correlation Techniques and Establishment of Volcanic Events

Correlating tephra layers between individual holes and sites is the foundation of our study, the establishment of an eruption chronology based on the marine tephra record. The correlations are primarily established on geochemical data (major and trace element compositions and their ratios) and stratigraphic relationships (vertically within the recovered sediment) between neighboring tephras. In addition, we compared the marine tephras by their visual appearance, for example macroscopically visible sedimentary structures, deposit colors, and grain size gradation. Before correlation, shipboard age models or previously published age models for the individual sites were applied, where applicable, and the approximate age of each tephra layer was calculated (see Section 5.1). At first, correlations were established between the individual holes of a drill site (e.g. between Holes C and D of Site 1124) by comparing the geochemical compositions (e.g. Figure 4) with respect to their calculated ages. If more than three to four geochemical values (majors, traces or ratios) do not overlap within the analytical error, a correlation is excluded (individual exceptions may occur). When a tephra correlation between individual holes was proven solid (by applying the above-mentioned criteria of e.g. age, geochemical homogeneity and visual appearance), we tried to find correlatives in closely neighboring drill sites. Subsequently, correlations to more distant drill sites were established.

Ultimately, all correlated and uncorrelated tephra layers are ascribed to volcanic events for which individual correlation codes are assigned (*s1–s69* for correlated, *u1–u139* for uncorrelated events; Table 1 and Table S1 in Supporting Information S2).

5. Results

5.1. Tephra Ages

The marine sediments and tephras were dated indirectly and directly. Indirect dating methods are based on shipboard age-depth models mostly derived from biostratigraphic and paleomagnetic data for each site (e.g. Barnes

Table 1
Key Major Elements and Trace Element Ratios for Correlated Marine Tephra Layers

Code	Sample ID	Age Ma	FeO_t wt%	SiO_2 wt%	Ba/La	Rb/Nd
s1	U1520D 55X-1 111-113	2.78	1.35	77.18	38.02	6.40
	1124C 8H-7 126-128		1.13	77.62		
s2	U1520D 55X-3 52-54	2.95	1.67	76.19		
	1124D 7H-3 63-65		1.57	76.90	36.98	5.99
	1125B 8H-2 70-72		1.58	76.65		
	1123A 12H-1 130-132		1.51	76.22	40.96	6.97
	594A 10X-6 6-8		1.64	76.22		
s3	1123C 11H-7 38-40	3.00	1.84	75.69	33.18	5.42
	1526A 3R-1 78-79		2.06	75.15		
s4	1124C 9H-3 17-19	3.09	1.40	76.26	41.04	6.98
	1124D 7H-5 54-56		1.43	76.42	40.48	6.59
	1123C 12H-2 74-76		1.43	76.59	41.52	7.22
	1123A 12H-3 56-58		1.37	76.33		
s5	1125B 9H-2 137-139	3.16	2.26	74.13		
	1125A 9H-5 90-92		2.30	74.30	32.19	5.80
	U1371D 7H-2 19-21		2.29	74.24	32.40	5.57
s6	U1520D 56X-1 28-30	3.18	1.82	75.75		
	1124D 7H-6 92-94		1.87	75.64	34.35	5.45
	1124C 9H-4 75-77		1.84	75.77	33.88	5.60
s7	1124D-7H-7 48-50	3.25	3.80	70.03	37.48	3.36
	1124C 9H-5 33-35		3.66	70.37	36.85	3.52
s8	1124D 8H-1 17-19	3.40	1.70	76.54		
	1124C 9H-6 68-70		1.74	76.33	29.19	4.26
	1123C 13H-4 67-69		1.77	76.45		
	1123A 13H-5 98-100		1.73	76.57	28.46	4.66
s9	1124C 9H-6 129-131	3.40	1.61	76.11		
	1124D 8H-1 73-75		1.57	76.47		
s10	1124C 9H-7 23-25	3.46	1.67	76.68		
	1124D 8H-1 117-119		1.65	76.70	29.09	4.80
	1123B 14H-2 4-6		1.63	76.55	28.91	4.57
s11	1124C 10H-1 97-99	3.58	2.15	75.21	30.33	5.50
	1124D 8H-3 96-98		2.08	75.34	30.14	5.40
s12	U1520D 58X-1 31-33	3.60	1.40	77.33		
	1124C 10H-1 124-126		1.20	77.20		
	1124D 8H-3 122-124		1.16	77.51	35.12	6.53
	1123B 14H-3 140-145		1.25	77.48	33.24	6.37
s13	1124C 10H-2 48-50	3.64	1.87	76.02		
	1124D 8H-4 45-47		1.90	75.75	32.01	5.31
	U1520D 58X-2 61-63		2.22	76.20		
*s14**	1123B 14H-5 72-74	3.68	2.58	73.26	30.01	5.32
	1123A 14H-3 90-92 I		2.70	73.10		
	1123A 14H-3 90-92 II		2.19	74.87	31.21	5.50

Table 1
Continued

Code	Sample ID	Age Ma	FeO_t wt%	SiO_2 wt%	Ba/La	Rb/Nd
s15	1124D 8H-5 2-4	3.70	1.47	77.20		
	1124C 10H-3 5-7		1.51	76.94	31.66	5.20
s16	1125B 11H-4 61-63	3.72	1.76	77.06		
	1125A 11H-7 52-54		1.73	77.22		
s17	1124D 8H-5W 120-122	3.77	1.08	77.59		
	1124C 10H-3 124-125		1.09	77.61	47.64	11.73
s18	1124D 8H-5W 136-138	3.78	2.74	73.67	25.60	4.90
	1124C 10H-3 141-143		2.81	73.35		
s19	1124D 8H-6W 4-6	3.79	3.19	72.75		
	1124C 10H-4 7-9		3.22	72.54	36.75	2.62
s20	1124C 10H-4 26-28	3.80	1.37	77.47	30.26	5.42
	1124D 8H-6W 25-27		1.39	77.34		
s21	1124C 10H-4 129-131	3.86	2.28	73.55		
	1124D 8H-6 128-130		2.24	73.56		
s22	1123B 15H-5 63-65	3.99	2.08	76.11	28.75	4.38
	1123C 15H-4 50-57		1.99	75.86	29.06	4.57
s23	1124D 9H-1 83-85	4.04	1.21	77.64	33.55	5.77
	1124C 10H-6 12-14		1.18	77.60	37.72	6.15
*s24**	1124C 11H-2 130-132	4.34	1.88	75.33	26.65	4.06
	1124D 9H-6 8-10 I		2.24	73.52		
	1124D 9H-6 8-10 II		1.29	77.42		
s25	1125B 15H-3 109-111	4.38	1.21	77.74		
	1125A 15H-6 142-144		1.27	77.97		
	1124C 11H-3 40-42		1.26	77.67		
	1124D 9H-6W 69-71		1.23	77.82	44.75	7.25
s26	1124C 11H-6 91-93	4.67	2.53	72.34		
	1125B 19H-4 47-49		2.90	71.37	26.65	2.17
s27	1124C 11H-7 30-32	4.72	3.07	73.93		
	1124D 10H-3W 109-111		3.05	73.76		
s28	1125A 20H-3 30-32	4.78	1.99	74.50		
	1124D 10H-4 66-68		2.09	74.90	28.87	2.16
*s29**	1124D 10H-5W 84-86 I	4.89	2.11	74.48		
	1124D 10H-5W 84-86 II		2.30	73.24		
	1124C 12H-2 35-37 I		2.37	73.35		
	1124C 12H-2 35-37 II		2.05	74.70	26.41	1.87
s30	1124D 10H-6W 23-25	4.94	1.25	77.23		
	1124C 12H-2 119-121		1.31	77.34	38.82	8.81
s31	1124D 10H-6W 57-59	4.95	2.79	72.54		
	1124C 12H-2 143-145		2.79	72.95	28.12	2.81
s32	1124D 11H-1 33-35	5.13	1.31	76.95		
	1124C 12H-4 141-143		1.34	76.64		

Table 1
Continued

Code	Sample ID	Age Ma	FeO_t wt%	SiO_2 wt%	Ba/La	Rb/Nd
*s33**	1124D 11H-1W 49-51 I	5.13	1.56	75.29		
	1124D 11H-1W 49-51 II		1.80	74.21		
	1124C 12H-5 5-7		1.74	74.71	28.76	3.18
s34	1124C 12H-5 103-105	5.20	1.04	78.12		
	1124A 11H-2W 13-15		1.01	78.18		
s35	1124C 12H-6 121-123	5.30	2.05	75.34		
	1124D 11H-3W 65-67		2.10	75.15	28.37	4.47
s36	1125B 24X-4 84-86	5.41	2.69	72.39	26.88	2.10
	U1520D 61X-2 42-43		2.57	73.36		
s37	1124C 13H-4 74-76	5.74	2.01	74.32		
	U1520D 63X-3 32-34		1.96	74.88	28.02	3.84
*s38**	1124C 13H-5 68-70	5.85	8.38	59.13	20.96	1.24
	1124D 12H-2W 139-141 I		10.63	53.85	30.34	2.45
	1124D 12H-2W 139-141 II		6.54	63.40	30.34	2.45
*s39**	1124C 13H-6 20-22	5.87	1.62	75.45		
	1124C 13H-6 24-26		1.28	76.95		
	U1520D 64X-1 69-71 I		1.48	76.79		
	U1520D 64X-1 69-71 II		2.05	74.45		
s40	1124C 13H-6 100-102	5.91	1.27	78.01		
	1124D 12H-3 28-30		1.30	77.67		
s41	1124C 13H-7 53-55	6.08	0.70	78.04	35.96	9.13
	1124D 12H-4W 25-27		0.73	78.18		
	1123B 24X-5 69-71		0.77	77.93	35.46	9.18
s42	1124C 14H-1 111-113	6.14	1.13	77.44		
	U1520D 64X-3 36-38		1.04	77.77		
s43	U1520D 65X-1 110-114	6.28	1.90	75.12	29.55	3.92
	1124C 14H-1 135-137		2.05	75.08	22.43	3.27
	1124D 12H-5W 133-135		2.03	75.09		
s44	U1520D 66X-2 88-90	6.34	2.89	71.39	25.85	3.02
	1124C 14H-6 122-124		2.97	71.35	50.92	2.44
	1124D 13H-4W 2-4		3.03	71.46		
s45	1124C 15H-2 119-121	6.83	0.79	77.84		
	1124D 13H-6W 135-137		0.79	77.87		
s46	1124D 13H-7W 53-55	6.87	2.31	71.90		
	1124C 15H-3 38-40		2.36	71.81		
s47	1124D 14H-1W 135-137	6.98	12.42	52.56	61.82	1.03
	1124C 15H-4 90-92		12.10	52.85	62.35	1.23
*s48**	U1520D 67X-1 83-85	7.00	2.51	74.50		
	1124D 14H-2 16-18 II		2.84	74.13	25.04	3.07
	1124D 14H-2 16-18 I		3.28	72.98		
	1124C 15H-4 106-108		3.18	72.94		
	U1520D 67X-1 91-92		2.64	74.09	27.00	3.92
	1124C 15H-4 141-143		2.43	74.64		

Table 1
Continued

Code	Sample ID	Age Ma	FeO_t wt%	SiO_2 wt%	Ba/La	Rb/Nd
	1124D 14H-2W 60-62		2.36	74.68		
*s49**	1124C 15H-5 38-40 I	7.05	2.17	74.34		
	1124C 15H-5 38-40 II		2.45	73.09		
	1124D 14H-2W 117-119		2.44	73.30	57.64	3.03
*s50**	U1520D 67X-1 115-116	7.06	2.18	75.66	26.35	4.33
	1124C 15H-5 69-71 II		2.21	75.37		
	U1520D 67X-1 116-117		1.60	76.50	38.15	6.88
	1124C 15H-5 69-71 I		1.58	76.51		
s51	U1520D 67X-CC 17-19	7.07	1.43	77.98		
	1124C 15H-5 101-103		1.44	77.67	25.81	3.47
*s52**	1124C 15H-5 131-133 I	7.11	2.88	74.08	26.66	3.76
	1124D 14H-3 76-78		2.76	73.85	28.03	3.99
*s53**	1124C 15H-5 131-133 II	7.11	1.68	76.70	26.66	3.76
	1124D 14H-3W 88-90		1.73	76.10		
s54	1124C 15H-6 35-37	7.14	1.05	77.31		
	1124D 14H-3 132-134		1.05	77.41	38.39	8.82
	594 36X-CC 10-12		0.98	77.27	30.41	6.97
s55	1125B 39X-3 136-138	7.30	2.52	75.18		
	1124C 16H-1 145-147		2.71	74.20		
	1124D 14H-6 35-37		2.74	74.16	23.07	3.48
s56	1124C 16H-2 18-20	7.36	1.46	75.72		
	1124D 14H-6W 51-53		1.53	75.55	23.07	2.21
*s57**	1124C-16H-2 115-117 I	7.42	1.93	75.67		
	1124C-16H-2 115-117 II		1.43	77.02		
	1124D 14H-7W 20-22		1.22	77.08	75.09	6.95
*s58**	1125B 40X-1 148-150 I	7.48	1.93	75.58		
	1124C 16H-3 134-136		1.76	75.26		
*s59**	1125B 40X-1 148-150 II	7.55	1.09	77.61	44.38	7.90
	1123B 29X-7 4-7		1.02	77.20	10.97	10.46
	U1371D 11H-3 51-53		1.01	77.39	9.98	9.76
s60	1124C 16H-4 130-132	7.59	2.66	74.26	20.01	1.80
	1123B 30X-3 100-102		2.77	74.17	22.21	2.05
	1125B 41X-5 22-24		2.71	74.15		
s61	1124C 17X-1 107-109	7.94	1.48	76.32	32.41	4.32
	1123B 31X-4 67-69		1.53	76.36	34.09	4.57
s62	1124C 17X-5 11-13	8.20/	0.98	77.85	34.73	7.74
	1123B 32X-2 87-89	8.28 ± 0.33	1.02	77.70	33.78	7.86
*s63**	1123B 32X-5 47-49 I	8.23	4.22	68.53	27.96	3.76
	1123B 32X-5 47-49 II		4.91	66.57	27.96	3.76
	1123B 32X-5 47-49 III		2.16	74.38	27.96	3.76
	U1520C-2R-2 31-34		2.10	74.70		
	1124C 17X-5 116-118		2.15	74.20	27.41	3.61

Table 1
Continued

Code	Sample ID	Age Ma	FeO_t wt%	SiO_2 wt%	Ba/La	Rb/Nd
*s64**	1124C 18X-5 136-138 I	8.90	2.34	73.20		
	1124C 18X-5 136-138 II		1.48	76.12	24.33	4.21
	1123B 34X-3 29-31		1.87	76.24	22.98	4.11
s65	U1520C 3R-2 70-72	8.98	1.82	75.55		
	1124C 18X-6 116-118		1.78	75.49		
s66	1125B 46X-3 72-74	9.45	0.94	78.10		
	U1520C 4R-1 0-2		1.11	78.21	23.14	4.59
s67	1125B 47X-4 65-67	9.53	1.83	75.84	27.17	3.19
	U1520C-4R-1 54-56		2.21	75.71		
s68	U1520C 8R-4 70-72	10.49	1.30	77.10		
	1125B 52X-5 117-19		1.26	77.62	27.69	4.69
	1123B 40X-6 119-121		1.27	77.44	28.15	5.58
s69	U1520C 8R-5 133-135	11.36/	0.99	77.20	20.86	12.36
	1123B 43X-1 77-79	11.9 ± 1.44	0.84	77.29	30.02	12.84

Note. These correlations correspond to 69 individual volcanic events (*s1* to *s69*). Volcanic events comprising bimodal or trimodal tephra layers (Sample ID plus "I," "II," or "III") are marked with an asterisk. Indicated ages per volcanic event are averages of indirect ages and, where applicable, direct U-Pb ages are given (*s62*, *s69*). We refer to the Table S1 in Supporting Information S2 for geochemical data, standard deviations and ages of individual marine tephra layers.

et al., 2019; Carter et al., 1999a, 1999b; Wallace et al., 2019). Direct dating relies on U-Pb zircon ages for selected marine tephra layers (Table 1 and Table S2 in Supporting Information S2), acknowledging that zircon crystallization recorded by these ages can predate tephra deposition. Where possible, indirect age models were verified or improved with direct U-Pb ages.

Indirect age constraints were converted into age-dependent sedimentation rates, which were ultimately used for the age calculation of marine tephra layers. Linear interpolation was applied between two key tephra horizons resulting in average sedimentation rates throughout the sediment record. This method has an uncertainty between 1% to 14% of their age, which is comparable to the analytical error of direct age methods like U-Pb dating or better (Kutterolf et al., 2013, 2021b). The thickness of the tephra layers was not corrected for, potentially leading to an overestimation of the sedimentation rates. In addition, sediment compaction and drilling disturbances, and possible small-scaled local reworking events cause difficulties in age calculations for different holes and sites leading to an over- or underestimation of the sedimentation rates. However, in line with previous contributions to the deep-sea drilling program, we chose to ignore corrections for the thickness of individual tephra layers, because their cumulative thickness of ∼30 m compared to ∼3,500 m total recovery (Quaternary and Neogene tephra record) is negligible, and the resulting ages would still be within the analytical error of direct dating methods.

The Quaternary age models for IODP Exp. 375 sites are well established and proceeding studies resulted in high-resolution age models (e.g. ^{14}C-dating; Barnes et al., 2019; Crundwell and Woodhouse, 2022b, 2022a; Woodhouse et al., 2022). Age models of the Neogene record of Exp. 375, however, have so far not been specifically addressed in preceding studies and we applied the shipboard age models for the calculation of the Neogene tephra record of Exp. 375 sites. In addition, few biostratigraphic marker horizons allowed to fine-tune the age model for tephras from Site U1520 (pers. comm. Martin Crundwell). For ODP Leg 181 Sites 1123, 1124 and 1125, Carter et al. (2004) established age models back to the Neogene and used a combined approach of paleomagnetic records, biostratigraphic datums, and an orbitally tuned benthic δ^{18}O record. These are assisted by glass isothermal plateau fission track ages from tephras of Site 1124. However, we found that previous studies use non-uniform depth units (meters below sea floor, "*mbsf*"; meters composite depths, "*mcd*"; revised meters composite depths "*rmcd*") without further explanation. In addition, the shipboard composite profiles of drill sites from ODP Leg 181 (Carter et al., 1999b), with revised depths and ages, were probably not applied. Implications are discussed in Section 7.1.

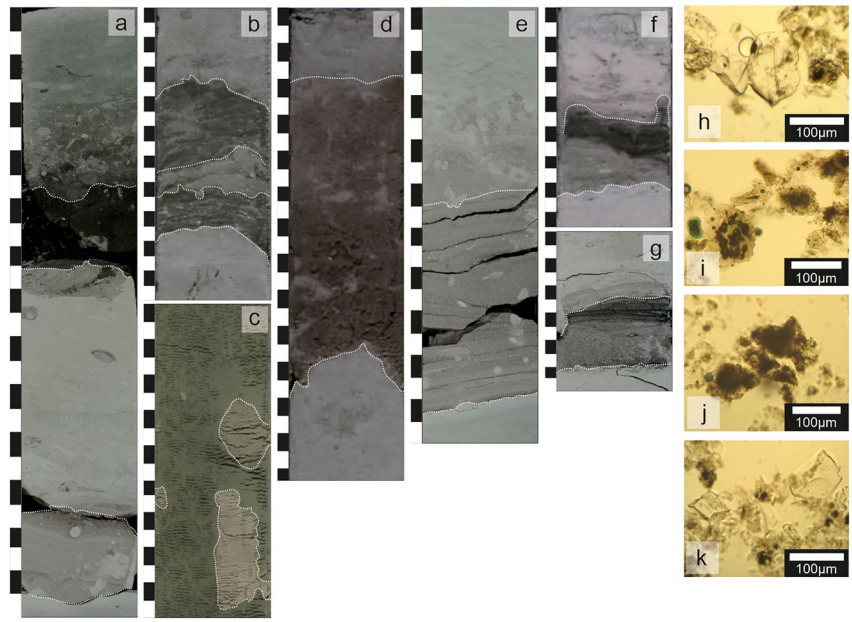

Figure 2. Examples of core sections with tephra layers (a–g) and glass shards (h–k) of marine tephra layers. Please see Table 1 and Table S1 in Supporting Information S2 for further explanations. (a) Two tephra layers in U1520C-8R-5, 68–94 cm: mafic tephra with bioturbation (upper layer, *u133*), and undisturbed rhyolitic layer (*u134*). (b) Rhyolitic tephra layer in 1125B-41X-5, 10–30 cm (*s60*) disturbed by drilling. Most likely the background sediment was squeezed into the tephra layer. (c) Tephra layer, rhyolitic, in U1371D-11H-3, 40–58 cm (*s59**) disrupted by drilling. (d) Sharp lower and diffuse upper contact of the rhyolitic tephra 1124C-16H-2, 0-27.5 cm (*s56*). (e) Light gray tephra U1520C-9R-2, 2–22 cm (*u136*) of rhyolitic composition. The tephra layer shows an internal structure (slightly changing colours and grain sizes) that resembles bedding. However, the sample was taken from the lowermost part of the bed, ensuring its original composition. Towards the top the tephra layer was bioturbated. (f) Rhyolitic tephra layer 1123B-24X-5, 60–75 cm (*s41*) with relatively sharp contacts to the surrounding sediment, a light gray colored base and black top. (g) Light gray, rhyolitic tephra layer U1520D-58X-1, 22–34 cm (*s12*) with a dark colored top. The upper contact shows signs of drilling disturbance. (h) Glass shard (left) with round vesicle in tephra U1520D-62X-2, 190 cm. (i) Brownish glass with many vesicles in sample U1520C-4R-5, 109 cm. (j) Glass shards in sample U1520C-11R-5, 63 cm. (k) Y-shaped glass shards with remnant bubbles in tephra layer U1520D-62X-2, 190 cm.

5.2. Tephra Inventory and Identification of Primary Tephra Layers

The recovered Neogene sediments of IODP Exp. 375 and ODP Leg 181 are mostly pelagic and transition to hemipelagic towards the top. All available intercalated and discrete tephra layers or pods were sampled. In addition, discrete and intact tephra layers or pods of selected sediment intervals of Site 594 and Site U1371 were included in this study.

The thickness of tephra layers varies from a few mm to several cm, but ash-pods or dispersed ash are present as well. The tephra layers occur in several colors (Figures 2a–2g) and the contacts to the surrounding sediments vary from sharp to wavy or diffuse, which are often the consequence of drilling or bioturbation, respectively (Figures 2a–2g; cf. Jutzeler et al., 2014). Analyzed glass shards are mostly fresh and transparent (Figures 2h and 2k), however in some older sediment intervals (e.g., Hole U1520C) the glass shards were slightly altered (Figure 2j). Intact and discrete tephra layers (Figures 2a and 2e) were not prioritized over disrupted or bioturbated tephra layers or pods (Figures 2b–2d).

The integrity of each individual tephra layer was screened intensely because only primary deposits are relevant for this study. The identification of primary tephra deposits is crucial because falsely identified primary tephra layers would increase the number of volcanic events during the Neogene. Vice versa, falsely identified reworked deposits would lower the number of total events. Therefore, the geochemical composition and visual appearance of each tephra layer was checked first individually and secondary within the stratigraphic context of the core and neighboring tephra layers.

Geochemically homogeneous, multi-modal or compositionally zoned tephra layers are considered primary if surrounding (vertically) tephra layers differ in visual appearance and geochemistry. Tephra layers with mixed

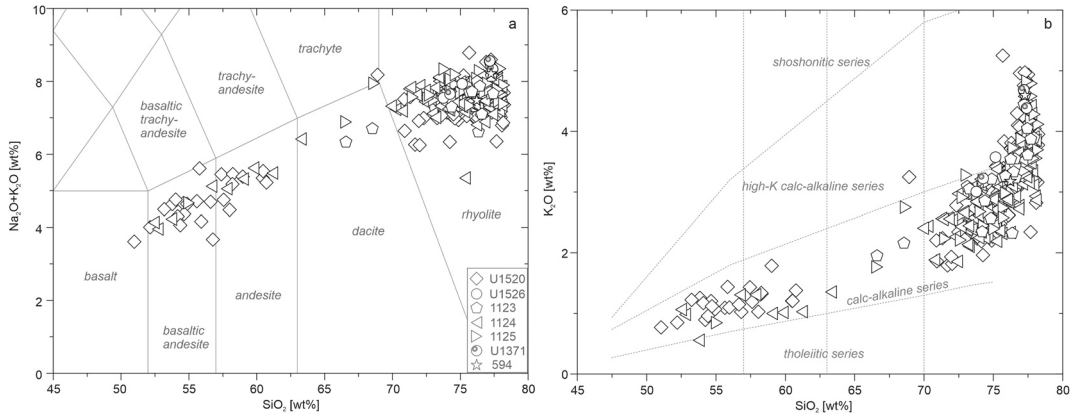

Figure 3. (a) Total alkali versus silica diagram after Le Maitre et al. (2002) showing the geochemical range of the primary marine tephra layers. Rhyolitic tephras clearly dominate at all sites, whereas basaltic to andesitic tephra layers are limited to Sites U1520, 1124 and 1125. Dacitic and trachytic compositions are rare (Sites U1520, 1123, 1124, 1125). (b) K_2O-SiO_2 classification diagram after Peccerillo and Taylor (1976). The majority of marine tephra layers follow the calc-alkaline trend, some rhyolitic glass shards with high silica (≥75 wt%) tend towards the high-K calc-alkaline series.

and genetically unrelated glass compositions are interpreted as reworked, especially when the tephra layers show visual signs of remobilization, for example, due to bioturbation and drilling disturbances. If tephra layers with the same geochemical composition and visual appearance occur repeatedly in sediment intervals, usually the lowermost or most discrete tephra layer is considered as primary, whereas the other tephra layers are characterized as reworked (exceptions may apply). The intense screening of each tephra layer, its surrounding sediment and vertically neighboring tephra layers, ultimately allows us to establish a robust tephrochronostratigraphy of New Zealand's Neogene explosive volcanism based on primary marine tephra layers, that were deposited either by fallout, vertical density flows, PDCs, or syneruptive tephra driven coastal mass transport continuing as submarine turbidites (Carey, 1997; Jutzeler et al., 2017; Manville & Wilson, 2004). Despite our multi-proxy approach to identify primary versus reworked deposits, it is possible that not all primary tephra layers were identified, or reworked tephra layers were mistakenly characterized as primary ones. However, due to the large number of investigated tephra layers in our study, our time series for the Neogene is still the most comprehensive to date.

402 ash-rich Neogene samples were recovered from the marine sediments and 306 of these are identified as primary. The primary tephras of the Neogene span a range from basaltic to rhyolitic compositions; however, the majority of tephras are rhyolitic with 73–78 wt% SiO_2 and 6.5 to 8 wt% $Na_2O + K_2O$ (Figure 3a). 33 tephras are basaltic or basaltic andesites with ~50–61 wt% SiO_2 and 3 to 6 wt% $Na_2O + K_2O$. Four tephras have a dacitic composition with 64–68 wt% SiO_2 and ~5.5 to 6.5 wt% $Na_2O + K_2O$ (Figure 3a). Two trachytic samples with ~69 wt% SiO_2 and ~8 wt% $Na_2O + K_2O$ were identified in Holes U1520C and 1125B.

On a $K_2O - SiO_2$ classification diagram (Peccerillo & Taylor, 1976), most marine tephras fall within the calc-alkaline field (Figure 3b). Tephras with highest silica compositions trend toward and/or plot within the high-K calc-alkaline series (Figure 3b).

5.2.1. Multi-Modal and Compositionally Zoned Marine Tephra Layers

26 tephra layers are identified as geochemically multi-modal characterized by two to three geochemical groups in at least one major/minor element. Volcanic events which include multi-modal tephra layers are highlighted with an asterisk ("*", Table 1 and Table S1 in Supporting Information S2). In addition, ~29 tephra layers with a zoned geochemical composition were identified. Compositionally zoned tephra layers are usually, but not exclusively, characterized by comparably heterogeneous compositions which form a geochemical trend in at least one major or minor element, resulting in exceptionally large standard deviations of >0.8 wt% (Table S1 in Supporting Information S2). Based on the overall integrity of these multi-modal and zoned tephra layers (e.g., visual appearance and unique geochemical compositions in stratigraphic context), we interpret them as primary. In addition, most of these tephra layers are correlated across the study area underlining their primary origin.

Of all identified multi-modal tephras 14 were correlated between holes and sites (*s14**, *s24**, *s29**, *s33**, *s38**, *s39**, *s48** - *s50**, *s52**, *s53**, *s57** - *s59**, *s63**, *s64**;* Table 1). The remaining twelve multi-modal tephras are

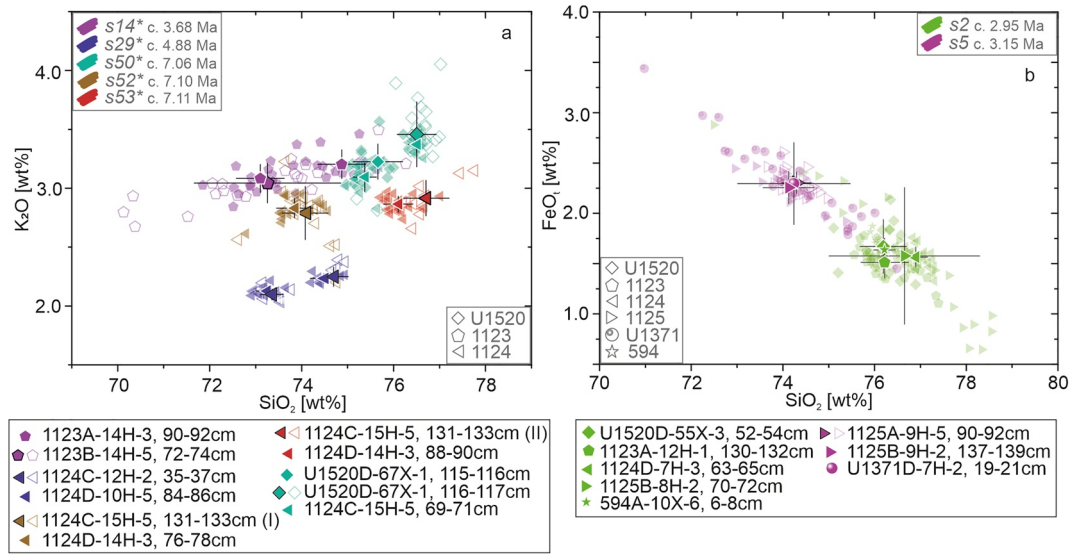

Figure 4. Examples of multi-modal volcanic events (a) and volcanic events with at least one compositionally zoned marine tephra layer (b). The colored and slightly transparent symbols (filled and open symbols) are single glass shard analyses and illustrate the overall geochemistry of correlated tephra layers. The larger symbols with error bars represent the average geochemical composition of the respective tephra layers.

uncorrelated, individual volcanic events (*u7**, *u11**, *u21**, *u29**, *u65**, *u101**, *u107**, *u119**, *u124**, *u126**; Table S1 in Supporting Information S2). Sometimes, only one geochemical group of a multi-modal tephra layer was successfully correlated, whereas the second or third geochemical group has a different composition which is not repeated in vertically neighboring tephra layers (e.g., *s64**). In other cases, one tephra layer spans the geochemical gap between correlated geochemical groups (e.g., *s24*, s38**).

In the following, some key correlated bimodal and compositionally zoned tephra layers are presented.

The youngest multi-modal volcanic event is *s14** (c. 3.68 Ma; Figure 4a; Table 1) correlated between a bimodal tephra layer from Site 1123 (1123A-14H-3, 90–92 cm) and a compositionally zoned tephra layer in the neighboring hole B (1123B-14H-5, 72–74 cm). The geochemical bimodality of this volcanic event is especially shown in SiO_2: the bimodal tephra has two compositional groups, one at 73.1 wt% SiO_2 (prominent group) and the second at 74.8 wt% SiO_2 (slightly less pronounced), whereas the zoned tephra is characterized by 73.2 ± 1.6 wt% SiO_2 (Figure 4a). The individual glass shard analyses of 1123B-14H-5, 72–74 cm show no prominent geochemical grouping but cover the entire compositional range of the bimodal tephra 1123A-14H-3, 90–92 cm. Volcanic event *s29** (c. 4.88 Ma; Figure 4a; Table 1) comprises the bimodal marine tephra layers 1124D-10H-5W, 84–86 cm and 1124C-12H-2, 35–37 cm. The bimodality is especially shown in SiO_2, TiO_2, K_2O and FeO_t. For example, the low-silica group (~73.3 wt% SiO_2) has 0.5 wt% TiO_2, 2.1 wt% K_2O and 2.3 wt% FeO_t, whereas the high-silica group (~74.6 wt% SiO_2) has 0.45 wt% TiO_2, ~2.23 wt% K_2O and ~2.08 wt% FeO_t (Figure 4a). Volcanic event *s50** is correlated across the study area between proximal Site U1520 (Hole D) and distal Site 1124 (Hole C) and is indirectly dated to 7.06 Ma (Table 1). In Hole U1520D, this volcanic event comprises a tephra layer that consists of two horizons which vary in color and geochemistry. The bottom part of the tephra layer (U1520D-67X-1, 116–117 cm) is of brownish color (~1 cm) with ~76.5 wt % SiO_2, 1.6 wt% FeO_t and ~3.5 wt% K_2O, whereas the upper part of the tephra layer (U1520D-67X-1, 115–116 cm) is gray-brown in color (~1 cm) with ~75.6 wt% SiO_2, ~2.2 wt% FeO_t and 3.2 wt% K_2O (Figure 4a). Its correlative is the bimodal tephra layer 1124C-15H-5, 69–71 cm with one compositional group at ~76.5 wt% SiO_2, 1.6 wt% FeO_t, 3.4 wt% K_2O, and the second group at ~75.4 wt% SiO_2, 2.2 wt% FeO_t and 3.1 wt% K_2O (Figure 4a). The volcanic events *s52** (c. 7.10 Ma) and *s53** (c. 7.11 Ma) are established between a bimodal tephra layer from Hole 1124C (1124C-15H-5, 131–133 cm) and two neighboring unimodal tephra layers from Hole 1124D (1124D-14H-3, 76–78 cm and 1124D-14H-3, 88–90 cm; Table 1), and are characterized by low silica compositions of ~74 wt% SiO_2 in volcanic event *s52** whereas *s53** has higher silica with ~76.5 wt% SiO_2 (Figure 4a). We believe that the bimodal character of the tephra in Hole 1124C is artificial, potentially caused by drilling disturbance, whereas in Hole 1124D, the geochemical signatures of both tephra layers remained intact.

Compositionally zoned tephra layers occur throughout the Neogene and many of these are uncorrelated with comparably low SiO_2 compositions (e.g., *u10*, U1520D-60X-1, 14–16 cm; *u42*, 1124D-13H-4W, 127–129 cm; Table S1 in Supporting Information S2). But, zoned low-silica rhyolites (e.g., *s26*) with ~71.3–72.3 wt% SiO_2 or medium-to high-silica rhyolites (e.g., *s2* and *s5*; Figure 4b; Table 1) with ~76 wt% SiO_2 and ~74 wt% SiO_2, respectively, occur as well.

The youngest compositionally zoned tephra layer was identified in Hole 1125B (*s2*, c. 2.95 Ma; Table 1). *S2* is correlated between five holes (Holes U1520D, 1123A, 1124D, 1125B and 594A; Figures 1a and 4b). The tephra 1125B-8H-2, 70–72 cm is zoned in SiO_2, Na_2O, K_2O and FeO_t. While silica increases from ~72.5 to 78.5 wt%, K_2O increases from ~2.5 to 4.3 wt%, whereas Na_2O (~5.3–3.7 wt%) and FeO_t (~2.9–0.6 wt%; Figure 4b) decrease. The correlative marine tephra layers are not classically zoned, but largely overlap with the mean composition of the zoned tephra (Figure 4b). Volcanic event *s5* also comprises a zoned tephra layer (U1371D-7H-2, 19–21 cm), which spans a compositional range from ~71 to 76.5 wt% SiO_2 with ~3.5 to 1.5 wt% FeO_t (Figure 4b). Its correlatives, two tephra layers from Site 1125, are comparably homogeneous (~74 wt% SiO_2 and 2.3 wt% FeO_t) and only the tephra layer from Hole 1125B shows a slight geochemical trend dependent mostly on silica and iron.

5.2.2. Distribution of Silica-Poor Tephra Layers

35 Neogene marine tephra layers are characterized by <70 wt% SiO_2, and thus geochemically differ from the vast majority of analyzed marine tephras with rhyolitic compositions (>70 wt% SiO_2; Figure 3). In total, these 35 silica-poor marine tephras correspond to 33 individual volcanic events (Table 1 and Table S1 in Supporting Information S2).

The majority of silica-poor marine tephras occur in the proximal Site U1520, with four volcanic events (youngest to oldest: *u10*, *u35*, *u37*, *u45*; Tables S1 and S7 in Supporting Information S2) between c. 4.99 Ma to 6.93 Ma in Hole U1520D, and 19 volcanic events between c. 8.21 Ma to 10.8 Ma in Hole U1520C (youngest to oldest: *u53*, *u69*, *u76*, *u82*, *u83*, *u85*, *u88*, *u94*, *u102*, *u103*, *u105*, *u107**, *u114*, *u115*, *u118*, *u121*, *u124**, *u132*, *u133*, *u135*; Table S1 in Supporting Information S2). One silica-poor volcanic event was identified in distal Hole 1123B (*s63**) and was indirectly dated at c. 8.4 Ma. Two volcanic events were identified in Hole 1125B (*u7**, *u131*) and were indirectly dated at c. 3.84 and 10.4 Ma. Another six silica-poor events are present between c. 5.0 to 8.02 Ma in Site 1124 (hole C: *u11**, *u48*, *u51*; holes C/D: *s38**, *s47*; hole D: *u42;* Table 1 and Tables S1, S9–S11 in Supporting Information S2).

The most continuous record of silica-poor explosive eruptions is preserved in the proximal marine Site U1520 (hole C) between 9.22 and 10.8 Ma.

6. Correlations of Marine Tephras

Geochemical fingerprinting allows for the correlation between volcanic deposits of unknown origin, such as marine tephra layers, because magmatic processes, for example, assimilation of continental crust or fractional crystallization, leave behind unique geochemical signatures (Lowe, 2011). These processes are stored in the major and trace element compositions of volcanic glass. However, for New Zealand's volcanism, it has been shown that the geochemical fingerprinting of volcanic deposits is not unambiguous but requires additional stratigraphic relationships and age constraints to produce confident correlations between volcanic deposits (Lowe, 2011). We therefore correlated the marine tephras using their geochemical fingerprint (major and trace element compositions, and trace element ratios), their stratigraphic contexts and site-specific age models, to establish (isochronous) tie-lines between the cores.

Following this approach, we established 168 tie-lines, correlating the marine tephra layers between holes and across the study area. The majority of correlations were established at Site 1124, followed by correlations at Sites U1520, 1123 and 1125. These 168 tie-lines of marine tephra layers between holes or sites correspond to 69 individual volcanic events (*s1* to *s69*; Table 1).

In the following, key correlations from youngest to oldest are highlighted.

The youngest identified volcanic event was correlated between the Holes U1520D and 1124C, and is indirectly dated to c. 2.77 Ma (*s1*). In Hole U1520D, *s1* consists of a ~3 cm thick tephra layer, whereas the thickness of

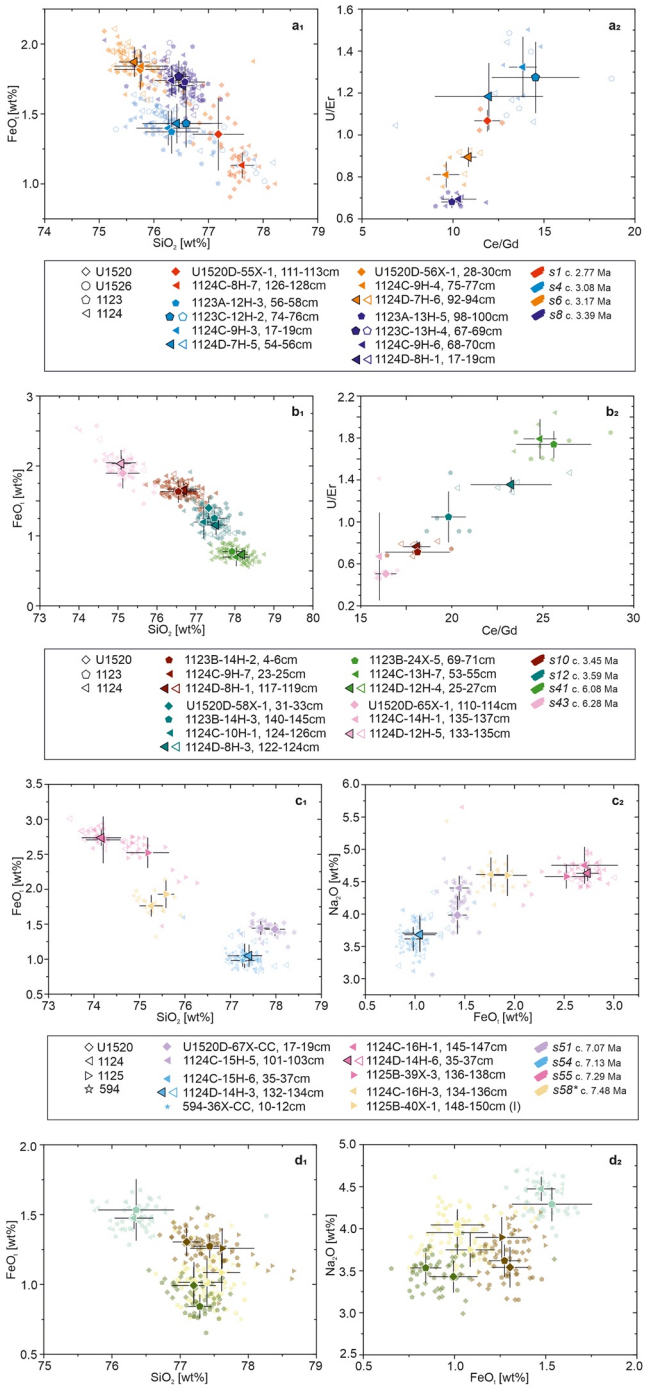

Figure 5. Harker (major and minor element compositions) and discrimination diagrams (trace element ratios) of Neogene tephra layers exemplarily showing correlations between sites ascribed to 16 volcanic events (*s1, s4, s6, s8, s10, s12, s41, s43, s51, s54, s55, s58*, s59*, s61, s68, s69*; Table 1). The slightly transparent symbols (open and filled) are single glass shard analyses, whereas larger symbols (filled, black and white frames) with error bars are geochemical averages. Please note, not all tephra layers were analyzed for trace element compositions (e.g. volcanic event *s1*, A_2).

the tephra in Hole 1124C is ~1 cm. The tephra is whitish to gray in color and characterized by comparably high silica compositions (~77.4 wt% SiO_2; Figure 5 A_1 and A_2). The second volcanic event (*s2*, indirectly dated to c. 2.95 Ma) was identified and correlated across the study area between Holes U1520D, 1123A, 1124D, 1125B and 594A. It is characterized for example, by 76.2–76.9 wt% SiO_2, 1.51 to 1.67 wt% FeO_t and 1.12 to 1.69 wt% CaO (Figure 4b). In Site 1124, for instance, volcanic event *s2* was identified as a ~5 cm thick gray to brown tephra layer, whereas in proximal Hole U1520D the color is brownish and the layer is slightly disrupted and <1 cm.

Four marine tephras, two from Site 1124 (holes C and D) and two from Site 1123 (holes A and C), were correlated and summarized in volcanic event *s4* (Table 1, Figure 5 A_1 and A_2). In Site 1124, this volcanic event formed a c. 10–15 cm thick brown tephra layer, whereas in the more distal Site 1123, only 2.5–5 cm of volcanic ash were deposited. Volcanic event *s4* is characterized by ~76.4 wt% SiO_2, ~1.4 wt% FeO_t, ~3.2 wt % K_2O, and comparably high U/Er (~1.2–1.3) and Ce/Gd (~12–14.5; Figure 5 A_1 and A_2). Volcanic event *s5* (c. 3.15 Ma) summarizes three marine tephra layers correlated between Site 1125 (holes A and B) and the southeasternmost Site U1371. It is the youngest Neogene volcanic event with ~74.2 wt% SiO_2, and comparably high FeO_t (2.3 wt%) and TiO_2 (~0.29 wt%) (Table 1). In Hole U1371D the tephra layer is compositionally zoned (Figure 4b), of brown color and ~2 cm thick. The volcanic event *s41*, indirectly dated to c. 6.08 Ma, was correlated between Hole 1123B and Site 1124 (holes C and D; Table 1). It is characterized by high SiO_2 (~78 wt%) and low FeO_t (~0.7 wt%; Figure 5 B_1), and high U/Er (~1.7) and Ce/Gd (17.3–18.1; Figure 5 B_2). In Hole 1123B, the marine tephra is ~5 cm thick with a light gray bottom and dark gray colored top (Figure 2f), whereas in Holes 1124C and D, the tephra layers are roughly 10 cm thick, with a dark gray colored base and a brown to beige colored top. Volcanic event *s54* is correlated across the distal sites of the study area between Sites 1124 (holes C and D) and 594 (Table 1). It is indirectly dated to c. 7.13 Ma and has high silica compositions (~77.6 wt% SiO_2) with low FeO_t (~1.05 wt%) and Na_2O (~3.7 wt%) (Figure 5 C_1 and C_2). In Holes 1124C and D, this volcanic event is characterized by <10 cm of beige to light brown volcanic ash. The volcanic events *s58** (indirect age: 7.48 Ma) and *s59** (indirect age: 7.54 Ma) are correlated between Holes 1124C and 1125B, and 1123B, 1125B and U1371D, respectively (Table 1). The marine tephra layer 1125B-40X-1, 148–150 cm is bimodal, with a low-silica group at ~75.6 wt% SiO_2 (*s58**; Figure 5 C_1) and a high-silica group at ~77.6 wt% SiO_2 (*s59**; Figure 5 D_1). The low-silica group is characterized by ~4.6 wt% Na_2O and ~1.8 wt% FeO_t, whereas the high-silica group has a lower Na_2O (~4 wt%) and FeO_t composition (~1.0 wt%; Figure 5 C_2 and D_2). In Hole 1123B this volcanic event is characterized by a light gray color with <2.5 cm thickness, whereas in Hole U1371D *s59** was identified as a disturbed beige colored tephra layer (Figure 2c). The oldest volcanic event, *s69*, was indirectly dated to c. 11.3 Ma and correlated between Holes U1520C and 1123B (Table 1). This volcanic event is characterized by ~0.9 wt% FeO_t compositions and ~4.75 wt% Na_2O (Figure 5 D_1 and D_2) at ~77.2 wt% SiO_2. Volcanic event *s69* deposited <2 cm of volcanic ash, varying in color from beige (Hole U1520C) to gray (Hole 1123B). Direct ages derived from U-Pb give an age of 11.9 ± 1.44 Ma for the marine tephra in Hole 1123B (Table 1), overlapping well with the indirect age.

6.1. Uncorrelated Marine Tephras

139 marine tephras could not be correlated, neither between holes nor sites, and each uncorrelated tephra layer is interpreted as an individual volcanic event (*u1* to *u139*; Table S1 in Supporting Information S2).

The majority of uncorrelated tephras are present in Site U1520 (95 marine tephra layers, 21 tephra layers in hole D and 74 in hole C). Most of these uncorrelated tephra layers occur between c. 10.8 Ma and 8.8 Ma (Hole U1520C), and thus represent the oldest continuous tephra record in our study (Figure 6). In Site 1124, we identified 24 uncorrelated marine tephra layers (hole C: 15, hole D: 9). The youngest uncorrelated tephra in Site 1124 was indirectly dated to c. 3.3 Ma (Hole 1124C) and the oldest to c. 17.4 Ma (Hole 1124C; Figure 6). 17 uncorrelated marine tephra layers were identified in Site 1125 (hole A: 2, hole B: 15). The youngest volcanic event in Site 1125 was indirectly dated to c. 2.6 Ma and the oldest to 10.4 Ma (Figure 6). In Hole 1123B, one uncorrelated tephra is present (c. 5.13 Ma). One uncorrelated tephra was identified in Hole U1526A indirectly dated to c. 3.04 Ma, and one in Hole U1371D indirectly dated to 8.09 Ma (Figure 6).

7. Discussion

7.1. Precision of Age Models

Neogene sediments with intercalated tephra layers were recovered from Site U1520 (Holes D and C), Site 1123 (Holes A, B and C), Site 1124 (Holes A, C and D), Site 1125 (Holes A and B), Sites 594 and U1371 (Figure 1a). For each drill site, age models have been determined by micropaleontology and paleomagnetism for the respective expedition (Section 5.1) and, where applicable, subsequent studies improved the indirect dated age-depth models by direct dating or detailed biostratigraphic work. This is, for example, the case for age models of ODP Leg 181 sites, revisited in previous studies (e.g. Alloway et al., 2005; Carter et al., 2004). The ages for sediments from Site U1520 and Hole U1526A are mostly based on shipboard age models of IODP Exp. 375.

Exemplary observations are discussed in the following.

1. Reported offsets between splices of sites and individual holes of ODP Leg 181 sediments were most likely not corrected for in subsequent studies (e.g. Allan et al., 2008) and are therefore difficult to translate to our study. We have corrected the tephra depths of individual ODP Leg 181 sites from the composite stratigraphy site depths by applying the given offsets in Carter et al. (1999a) and as a result observed slight to significant age shifts. For example, the offset in the sediment interval where tephra layer 1123A-12H-1, 130–132 cm (*s2*; Table 1) occurs is an addition of +7.84 m to the mbsf-depths of each intercalated tephra layer in the sediment interval between 101.1 and 110.63 mbsf. This correction leads to an age of 3.05 Ma (with offset correction), whereas the age without offset-correction would be 2.84 Ma. Another example is volcanic event *s14** (Table 1), correlated between the marine tephras 1123A-14H-3, 90–92 cm and 1123B-14H-5, 72–74 cm. Without offset-correction from the composite depth, indirect dating of these tephra layers results in c. 3.43 Ma (Hole 1123A) and 3.43 Ma (Hole 1123B). With offset-correction, however, they are ∼260 ka older and the individual ages result in 3.69 Ma (Hole 1123A; addition of +9.88 m in the sediment interval between 120.1 and 129.54 mbsf) and 3.66 Ma (Hole 1123B; addition of +8.6 m for the sediment interval between 117.4 and 126.88 mbsf). In general, the resulting age differences between offset-corrected and uncorrected ages increase with increasing depths of the sediments from <100 ka (interval: 0 to 50 mbsf) to c. 230 ka to c. 350 ka (interval: ∼118 to 290 mbsf) or even 411 ka (interval: ∼310 to 395 mbsf) for the deepest tephra layers in Hole 1123B. A direct comparison to previous studies focusing on Neogene tephras (Carter et al., 2004) is difficult because these authors do not refer to sampling depths of the tephras but use their own nomenclature. However, comparisons to the Quaternary tephra record show that the established ages for tephras studied in Carter et al. (2004) and Allan et al. (2008) differ from our calculations. For example, the marine Quaternary tephra 1123B- 5H-3, 3–5 cm has an offset-corrected age of c. 857 ka. Its age without offset-correction is c. 792 ka and Allan et al. (2008) report an age of c. 991 ka. Based on the publicly available data, we were not able to ultimately resolve this issue. However, the resulting age differences are generally within the analytical error of direct dating methods, thus not relevant for the correlation purpose of this study, although it is important to use the consistently calculated corrected tephra ages in further studies.
2. A missing isotopic cycle in Site 1123 leads to an addition of 2.72 m to all data from sediment intervals deeper than cores 5H from Holes 1123A, 1123B and 1123C. Starting at cores 8H at Holes 1123C as well as 9H at Hole 1123A and 1123B an addition of 0.14 m to the cores is added on top of the previous given extensions (Hall

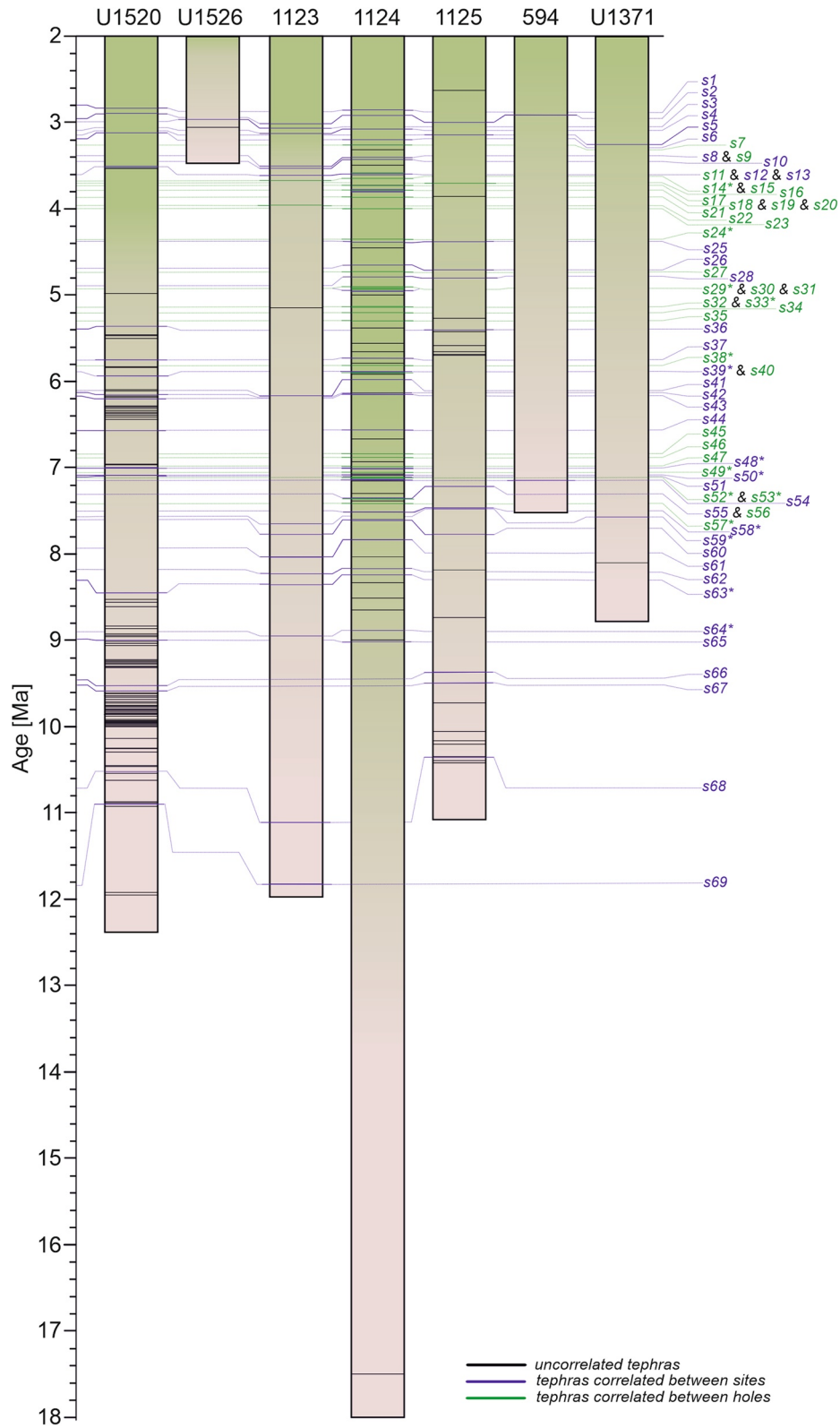

Figure 6. Core profiles of Sites U1520, U1526, 1123, 1124, 1125, 594 and U1371 showing the individual Neogene tephra layers, uncorrelated (black), correlated between holes (green) and between sites (blue) in hemipelagic (green) to pelagic (light pink) background sediment. Explanations of correlation codes (*s1* to *s69*) are given in Table 1, labels for uncorrelated tephras (*u1* to *u139*, Table S1 in Supporting Information S2) are not shown.

et al., 2001; Harris, 2002). When applying these additional depth corrections, the re-calculated ages of marine tephras vary strongly from previously established age-depth constraints, with or without offset-correction, and become older, for example, from 8.93 Ma to 9.03 Ma (1123B-34X-3, 29–31 cm, *s64**; Table 1). This age shift alone would not be a problem, but the effects on established site to site correlations in the region (previously or within this study), for example, between Sites 1123 and 1124, are large. Previous studies (e.g., Allan et al., 2008; Carter et al., 2004) refer to these corrections proposed by Hall et al. (2001) and Harris (2002). However, their indirect ages do not include the depth adjustments after Hall et al. (2001) and Harris (2002). Thus, we decided to follow their example and did not explicitly apply the corrections. Re-visiting previously and newly established correlations between ODP Leg 181 sites, in combination with direct zircon ages (this study, Table S1 and S2 in Supporting Information S2), support our approach.

3. Direct U-Pb age dating of zircons was carried out for five Neogene marine tephra layers (Table 1 and Tables S1 and S2 in Supporting Information S2). For example, marine tephra 1123B-32X-2, 87-89 cm (*s62*, Table 1) was indirectly dated to 8.24 Ma (without offset-correction 7.91 Ma) and its direct U-Pb zircon age resulted in 8.28 ± 0.33 Ma, more closely aligned with the age assigned when the offset-correction is applied. This volcanic event was correlated to a tephra layer in Hole 1124C (1124C-17X-5, 11–13 cm) indirectly dated to 8.16 Ma, thus slightly younger than the proposed indirect age of this volcanic event in Hole 1123B, but still within the analytical error of the direct U-Pb zircon age. For Site U1520, however, the Neogene shipboard age model was less well constrained, leading to an offset of up to 2.5 Ma for the deepest tephra layers between the indirectly calculated ages and direct U-Pb zircon ages. Here, we adjusted the age-depth model by applying our direct U-Pb zircon ages and newly revised biostratigraphic datums (M. Crundwell, pers. comm.), resulting in a most robust age model for the Neogene sediments at Site U1520 to date.

7.2. Preservation of Marine Tephras

The drill sites cover a wide study area east to southeast to south of New Zealand and thus enable to establish first constraints regarding tephra dispersal and tephra preservation during the Neogene. Strogen et al. (2022) show the tectonic evolution of the continent of Zealandia and suggest that at 19 Ma our study sites in the East Coast Basin (Sites U1520 and U1526) would have been closer to the CVZ and Northland arc source volcanism than today. Between 19 and 10 Ma, the East Coast Basin rotated clockwise away from the CVZ and Northland arc sources, and by 10 Ma the sites would have been close to their present-day locations (Strogen et al., 2022). Rifting of the TVZ occurs since c. 2 Ma and increases the distance between volcanic source and IODP Exp. 375 drill sites; however, these small-scale plate motions are negligible for the purpose of this study. The drill sites from ODP Leg 181 are located on the incoming Pacific Plate, which is subducted beneath North Island (New Zealand) since at least 20 Ma. The plate reconstructions from Strogen et al. (2022) imply that, for example, Site 1124 would have been located ∼650 km further to the east from its present-day location at c. 10 Ma. Between c. 10 and 4 Ma, the distance generally decreases but at c. 4 Ma, Site 1124 would still have been ∼300 km to the east from its present-day location (Strogen et al., 2022). Our oldest tephra layers from Site 1124 have therefore been deposited in sediments ∼900 km more distal than today. This observation, which affects all distal drill sites, is considered in our discussions below.

Most marine tephras, correlated or uncorrelated, were identified in Site U1520 (116 tephra layers; at present c. 104 km E from Gisborne; Figure 1a) and Site 1124 (127 tephra layers; at present c. 486 km E from Gisborne), and to a lesser extent in Site 1125 (35 tephra layers; at present c. 540 km SE from Gisborne) and Site 1123 (22 tephra layers; at present c. 960 km SE from Gisborne). The tephra layers in Site U1520 occur between c. 2.68 Ma and c. 11.9 Ma with the highest concentrations between c. 6.1 to 6.4 Ma, and between c. 8.8 to 10.8 Ma (Figure 6). The latter time interval in Site U1520 is the oldest continuous Neogene tephra record present in our study (Figure 6). In comparison, the oldest continuous tephra record in Site 1124 ends at c. 9 Ma, in Site 1125 it extends to c. 10.5 Ma, whereas Site 1123 does not contain a continuous record but more sporadic tephra occurrence back to c. 11.8 Ma (Figure 6). For Site 1124, intensified deposition of volcanic material is observed between c. 3 to 9 Ma, resulting in a continuous tephra record during that time period (Figure 6). These changes in tephra occurrence between the individual drill sites are most likely explained by re-arranging plate boundaries and plate motions during the Neogene (Carter et al., 2004; King, 2000; Strogen et al., 2022), (a) potentially hindering volcanic material reaching the depositional areas, (b) potentially favoring the deposition of volcanic material at one location over another, and (c) generally limiting the deposition of fallout at the very distal drill sites of ODP Leg 181 to only very large eruptions. An alternate explanation could be variations in dominant paleowind directions with

time, leading to local accumulation (e.g. at Site 1124) or absence (e.g. at Sites 594 and U1371) of tephra layers in the marine sediments. Most likely both factors played a fundamental role in the distribution of volcanic material towards the marine environment east and southeast of New Zealand.

Marine tephra layers in the most southwestern Site 594 and southeastern Site U1371 are condensed in two intervals, between c. 2.9–3.1 Ma and between c. 7.1–8.08 Ma. At c. 2.95 Ma and 3.15 Ma two volcanic events are preserved at Sites 594 (*s2*) and U1371 (*s5*), then ∼4 Myr pass without a single marine tephra layer in both sites in our tephra records. At c. 7.1 Ma we identified a tephra layer in Site 594 (*s54*), followed by two volcanic events forming marine tephra layers at U1371 (*s59** and *u52*), indirectly dated to c. 7.54 Ma and c. 8.09 Ma, respectively (Figure 6, Table 1 and Table S1 in Supporting Information S2). These marine tephras reaching the southwesternmost and southeasternmost study areas might be the deposits of exceptionally large eruptions similar to the recent Kawakawa/Oruanui super eruption that deposited volcanic ash as far as Antarctica (Dunbar et al., 2017). Examples from large eruptions of the Central American volcanic arc and the Japanese arcs show that those eruptions are able to influence and even modify or suspend the prevailing wind regimes even up to the stratosphere and therefore also the dispersal of ash in the known distribution pattern of smaller eruptions (e.g. Brenna et al., 2021; Cisneros de León et al., 2021). However, the thicknesses of respective tephra layers within the cores do not differ significantly, if at all, from other tephra layers, excluding this assumption. An alternate hypothesis for these periods of heightened tephra preservation is changes in the paleowinds transporting volcanic ash more dominantly towards the SW and SE of New Zealand. Both time intervals, between c. 2.9–3.1 Ma and between c. 7.1–8.08 Ma, are present in both distal drill sites, likely indicating the deposition of these tephra layers while the prevailing wind directions were unstable and changing.

7.3. Spatiotemporal Compositional Variations and New Insights Into the Geochemical Evolution From CVZ to TVZ Volcanism

Next to the above discussed dispersal of volcanic material and probable changes in paleowinds, the extensive tephra record allows for a spatiotemporal geochemical comparison of the marine tephra layers present in the drill sites.

7.3.1. Spatiotemporal Compositional Variations

Generally, the marine tephra record from all drill sites show that New Zealand's Neogene explosive volcanism mainly produced silica-rich volcanic material of rhyolitic composition with only a few geochemical exceptions being silica-poor to mafic (Figure 3a).

We found that most silica-poor (<70 wt% SiO_2) volcanic events of the Neogene are present in the proximal Site U1520, and sporadically present in the distal Sites 1124, 1125 and 1123 (see Section 5.2.2). The high abundance of silica-poor tephras in the proximal Site U1520 is most likely explained by the site's proximity to the volcanic source in the CVZ because dense silica-poor tephra is not likely to travel as far as silica-rich tephra leading to a natural accumulation of silica-poor tephra closest to source (e.g. Pearce et al., 2020).

During the late Pliocene (c. 3.8 to 2.58 Ma) silica-poor marine tephra layers are absent in the marine sediments, except for one volcanic event at c. 3.84 (*u7**) present in Site 1125. Between c. 4.9 Ma to c. 8.2 Ma silica-poor volcanic events are equally rare, but present at c. 4.99 Ma (*u10*, Hole U1520D), c. 5.0 Ma (*u11**, Site 1124), c. 5.84 Ma (*s38**, Site 1124), c. 6.33 Ma (*u35*, Hole U1520D), c. 6.36 Ma (*u37*, Hole U1520D), c. 6.65 Ma (*u42*, Site 1124), c. 6.93 Ma (*u45*, Hole U1520D), c. 6.98 Ma (*s47*, Site 1124), c. 7.28 Ma (*u48*, Site 1124), c. 8.02 Ma (*u51*, Site 1124), c. 8.21 Ma (*u53*; Hole u1520D), and c. 8.23 Ma (*s63**, Site 1123; Table S1 in Supporting Information S2). These volcanic events are characterized by varying silica compositions between ∼51–66.4 wt% SiO_2 (Table S1 in Supporting Information S2). Between c. 8.2 Ma to 9.2 Ma silica-poor volcanic events are absent again, before they become abundant and continuous until c. 10.8 Ma (Table S1 in Supporting Information S2). The volcanic events during this 1.6 Myr time interval are characterized by low silica compositions mostly ranging between ∼52.1 - 58.2 wt% SiO_2 (except for four volcanic events with ∼60.4 to 68.9 wt% SiO_2). The temporal distribution of silica-poor tephra in the marine record is most continuous between c. 9.2 to 10.8 Ma and might reflect the overall geochemical evolution of the CVZ from a more mafic volcanic arc toward a more evolved silicic arc. An alternate explanation is an overall increased incidence of explosive silica-poor eruptions during the early stages of CVZ volcanism, large enough to reach the submarine depositional areas. The absence of silica-poor volcanic events during shorter time periods, for example between c. 8.2 to 9.2 Ma, might be explained by local rearrangements between volcanic centers, maybe associated with fewer explosive eruptions.

Between c. 10.2 and 9.6 Ma, silica-poor volcanic events are most frequent in the marine tephra record (Table S1 in Supporting Information S2) and their abundance implies that mafic explosive eruptions occurred every ∼12 Kyr within this time interval. A more detailed study about eruption frequency, with regard to silica-poor volcanism, eruption magnitudes and potential climate interactions, will be addressed in a future study by the authors.

7.3.2. Geochemical Evolution From CVZ to TVZ Volcanism

The established detailed marine tephrochronostratigraphy allows preliminarily investigation into the temporal compositional variations within the respective record of New Zealand's volcanism.

Three periods of lower abundances of marine tephra layers from the Miocene to the Pleistocene are identified in our records (Figure 7). These are in the Late Miocene (9–8.5 Ma), the Middle Pliocene (4.7–4 Ma), and between the Pliocene and Pleistocene (2.9–2.5 Ma). This reduced tephra abundance in the marine sediments may be due to an incomplete tephra record within these time intervals but also due to fundamental changes in the arc systems like local and regional tectonic rearrangements or global climate (e.g. Kutterolf et al., 2019; Schindlbeck et al., 2018a), which must be further investigated. Next to these times of quiescence, compositional trends are observed that may be related to either general trends of New Zealand's subduction systems, changes between the arc systems with time, or contribution from other volcanic sources. Tentative interpretations can be made on the base of the variations within trace element ratios regarding increasing or decreasing fluid and/or crustal contamination/interaction or variable melting degree (e.g., crust: Chen et al., 2020; Walker et al., 2007; Waight et al., 2017; fluids: Bolge et al., 2009; Carr et al., 1990; Elliott, 2003; Plank, 2014; Zamboni et al., 2016; melting degree: Münker, 2000; Pfänder et al., 2012; Zirakparvar, 2016).

1. Starting in the early Late Miocene (11 Ma) until the second and most pronounced gap in our tephra record, two (Figure 7c) to three (Figure 7e) distinct compositions can be identified within the tephra time series possibly indicating a different volcanic source for the related tephras associated with higher fluid (Figure 7c) and lower crustal (Figures 7e and 7f) interaction. This may be evidence for either an ultra-distal volcanic source (e.g. Smith et al., 2016) for example one decoupled from the overall New Zealand subduction zone magmatism, or it represents a source that is placed behind the arc present in the respective time interval, facilitating a different fluid contribution to magma generation and less pronounced access to crustal contamination. In the scope of the regional tectonic setting as well as the thicknesses and grain sizes of the ash layers an ultra-distal volcanic source can be excluded and the second latter interpretation seems favorable. This group of different tephra compositions within this oldest time interval is accompanied by tephra layers with compositions that follow a similar trend/composition than shown by tephra related to the Taupō Volcanic Zone.
2. From the Late Miocene on, one can identify pronounced (Figures 7a, 7b and 7d) to vague (Figures 7c, 7e and 7) continuous compositional trends within the entire tephra time series. An increasing signal of crustal interaction is paralleled by a decreasing degree of melting (Figures 7a, 7b, 7d and 7f).
3. The tephra compositions after the 0.7 Ma gap in the Middle Pliocene towards the Pleistocene have overall higher Li/Y, La/Yb, La/Sm, Nb/Yb and lower Zr/Rb ratios, indicating an overall decreasing signal of fluids and melting degree at the time with increasing influence of crustal interaction (Figures 7a, 7b, 7d–7f).
4. Considering the geochemical signatures of the trace element ratios with time (Figures 7a, 7b and 7d), it seems that after a short period of volcanic quiescence at c. 4.5 Ma, the geochemical signature changed towards more TVZ-like compositions, potentially indicating that the geochemical transition from CVZ to TVZ started at around that time. This geochemical shift may be correlated with major changes in the degree of melting and crustal interaction as described above.

7.4. Neogene Tephrochronostratigraphy and Repose Times

The marine tephra record of the Neogene presents intervals with increased numbers of intercalated marine tephra versus intervals of tephra absence within the marine sediments, which might be an indicator for increased explosive volcanic activity compared to no or only very few volcanic events (Figure 6). Overall, four main intervals with varying eruption frequencies were identified and allow for a first holistic estimation of repose times for New Zealand's Neogene volcanism (Figure 8; Table S14 in Supporting Information S2).

The oldest interval with fewest tephra abundance in the marine sediments is between c. 11.9 Ma and 10.6 Ma with one eruption occurring approximately every 310 Kyr (Figure 8). This number is most likely not representative for New Zealand's volcanism at that time, since onshore records indicate continuous volcanic activity (e.g.

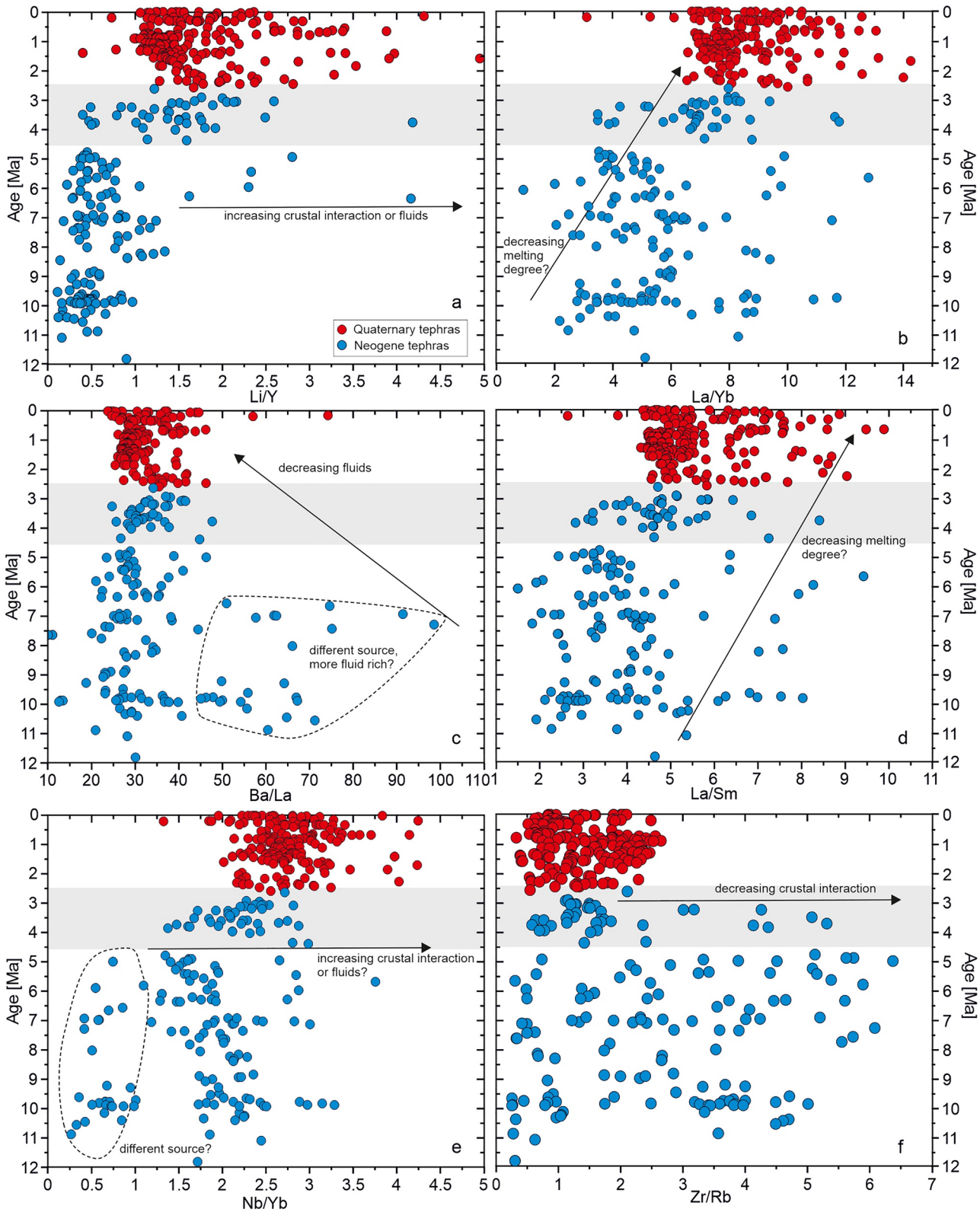

Figure 7. Geochemical evolution from the Neogene (blue circles) and the Quaternary (red circles) based on the marine tephra record. Quaternary marine tephra data from Pank et al. (2023). The gray bar extends from c. 4.5 to 2.5 Ma and probably represents a time of geochemical transition from CVZ to TVZ. Other volcanic sources contributing to the marine sediments are possible, as indicated by varying trace element compositions and ratios of some marine tephras between c. 11 to 5 Ma.

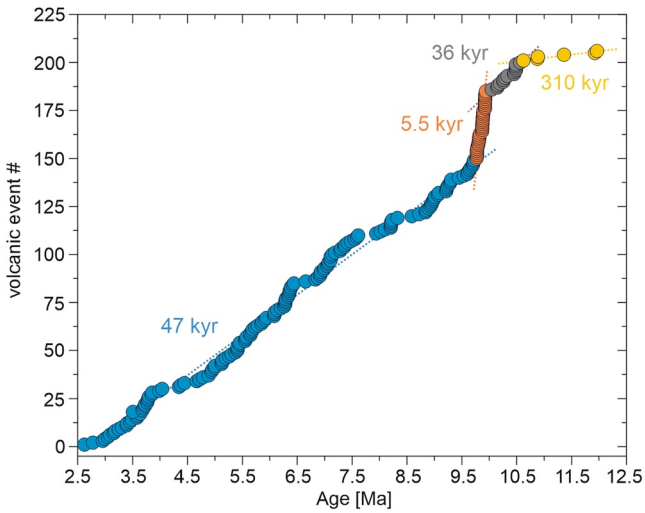

Figure 8. Repose times of New Zealand's explosive volcanism during the Neogene based on the marine tephra record. Four intervals (yellow, gray, orange and blue) with varying repose times over time were identified (e.g., between c. 9.6 Ma to 2.6 Ma one eruption occurred every 47 yr). Please find the calculations in Table S14 in Supporting Information S2.

Booden et al., 2012). We believe that the marine tephra inventory during this interval is incomplete, probably due to the distance between volcanic source and drill sites, and that the calculated repose time represents a maximum value. From c. 10.5 to 2.6 Myr the marine tephra record indicates continuous explosive volcanic activity with frequent tephra layers mostly in Sites U1520 and 1124 (Figure 6). Calculated repose times reveal that for the interval between c. 10.5 to 10.0 Ma one eruption occurred approximately every 36 Kyr, and for the interval between c. 9.7 to 2.6 Ma slightly longer repose times with one eruption occurring every 47 Kyr (Figure 8). Between c. 9.9 to 9.7 Ma, however, the calculated repose times are significantly shorter with one eruption occurring every 5.5 Kyr (Figure 8). During this time interval of c. 200 Kyr 38 volcanic events are present at Site U1520, probably indicating a short period of increased volcanism with comparably small eruptions only reaching the most proximal marine drill site.

The calculated repose times give insights into New Zealand's Neogene explosive volcanism, but should be considered as maximum intervals of recurrence because the marine tephra record most likely lack deposits of small explosive and effusive eruptions. However, compared to previous studies from Carter et al. (2003) and Stevens (2010) where the authors propose one eruption per 163 Kyr (Carter et al., 2003) and one per 99 Kyr (Stevens, 2010) for the Miocene and one eruption per 86 Kyr and one per 74 Kyr during the Pliocene, our repose times are the most accurate and detailed to date, revealing better variabilities over time, but overall are comparable and within the same order of magnitude.

8. Conclusions

We established a comprehensive tephrochronostratigraphy for New Zealand's Neogene volcanism based on marine tephra layers from IODP Exp. 375, ODP Leg 181, IODP Leg 329 and DSDP Leg 90, covering the proximal and distal marine environment to the east and southeast of North Island, New Zealand.

All ash-rich samples were analyzed for their major element compositions, and selected samples were further analyzed for trace element compositions, resulting in a geochemical fingerprint for each marine tephra. We combined the geochemical fingerprints, with the stratigraphic context and indirect and/or direct ages of each marine tephra layer, and identified 306 as primary. Correlations between marine tephra layers from individual holes and sites revealed 168 tie-lines, corresponding to 208 Neogene volcanic events. Of these, 69 were identified in several holes/sites (*s1* to *s69*), whereas the other 139 marine tephras are single hole or site-specific tephras (uncorrelated volcanic events *u1* to *u139*).

The marine tephra record is continuous until c. 12 Ma, with one additional volcanic event at c. 17.5 Ma (Site 1124). The most continuous tephra record was identified in Site 1124 between c. 2.8 to 9 Ma, whereas the tephra record from Sites U1526, 1123, 1125, 594 and U1371 are fragmentary but complementary, partly filling gaps or extending the record. In Site U1520 the tephra record is continuous between c. 5.8 to 6.5 Ma and between c. 8.8 to 10 Ma but fragmentary outside these intervals. Repose time calculations during the Neogene reveal four intervals with one eruption every 310 Kyr between 11.9 Ma and 10.6 Ma, one eruption every 36 Kyr between 10.5 Ma and 10.0 Ma, one eruption every 5.5 Kyr between 9.9 Ma and 9.7 Ma, and one eruption every 47 Kyr between 9.7 Ma and 2.6 Ma.

The preservation of marine tephra layers in different drill sites (proximal or distal) reflects plate motions since the Neogene and associated distances between volcanic source and depositional area, but also allows the interpretation of changes in paleowind directions with time. The preservation of tephras in the sediment record also allows for a general interpretation of phases with increased volcanic activity versus phases with decreased volcanic activity. These phases will be compared and contrasted with existing knowledge of the volcanic activity of the TVZ in a future study by the authors to investigate patterns in eruptive behavior with regard to climatic events.

The marine tephra layers of the Neogene span a compositional range from rhyolitic to basaltic, which has not been described before for New Zealand's Neogene explosive volcanism. In addition, some geochemical parameters,

for example contamination specific trace elements and their ratios, show an abrupt geochemical change from c. 4.5 Ma on, likely related to the transition from the Neogene volcanic system (CVZ) to the Quaternary volcanic system (TVZ).

Data Availability Statement

All raw data of geochemical microanalyses are published in the IODP Proceedings of IODP Exp. 372/375 in Pank et al. (2023).

Acknowledgments
The samples of this study were provided by the International Ocean Discovery Program (IODP) as well as Ocean Drilling Program (ODP) and Deep Sea Drilling Project (DSDP). The excellent efforts of all participating on- and offshore technicians, lab leading officers and crew, the drilling personnel, and all scientific parties are greatly acknowledged. Funding for this research was provided by the German research foundation (DFG), associated to the DFG IODP priority program, by the grant KU2685/11-1 and 11-2. J.L. Hopkins acknowledges the NZ Marsden Fund Te Pūta Rangahau a Marsden for supporting her Marsden Fast Start project, "Cryptotephra: unearthing hidden eruptions from the Taupō Volcanic Zone" (MFP-VUW1809). The authors wish to acknowledge funding support from L. Strachan's NZ Marsden Fund Te Pūta Rangahau a Marsden project, "Does climate influence the frequency of volcanic activity and earthquakes?" (MFP-20-UOA-099). The authors greatly acknowledge constructive and thorough reviews of Adrian Pittari and an anonymous reviewer. Open Access funding enabled and organized by Projekt DEAL.

References

Adams, C. J., Graham, I. J., Seward, D., Skinner, D. N. B., Moore, P. R., & Moore, P. R. (1994). Geochronological and geochemical evolution of late Cenozoic volcanism in the Coromandel Peninsula, New Zealand. *New Zealand Journal of Geology and Geophysics*, *37*(3), 359–379. https://doi.org/10.1080/00288306.1994.9514626

Allan, A. S., Baker, J. A., Carter, L., & Wysoczanksi, R. J. (2008). Reconstructing the Quaternary evolution of the world's most active silicic volcanic system: Insights from an ∼1.65Ma deep ocean tephra record sourced from Taupo Volcanic Zone, New Zealand. *Quaternary Science Reviews*, *27*(25–26), 2341–2360. https://doi.org/10.1016/j.quascirev.2008.09.003

Alloway, B. V., Pillans, B. J., Carter, L., Naish, T. R., & Westgate, J. A. (2005). Onshore–offshore correlation of Pleistocene rhyolitic eruptions from New Zealand: Implications for TVZ eruptive history and paleoenvironmental construction. *Quaternary Science Reviews*, *24*(14–15), 1601–1622. https://doi.org/10.1016/j.quascirev.2004.07.026

Barnes, P. M., Wallace, L. M., Saffer, D. M., Pecher, I. A., Petronotis, K. E., LeVay, L. J., et al. (2019). Site U1520. In L. M. Wallace, D. M. Saffer, P. M. Barnes, I. A. Pecher, K. E. Petronotis, & L. J. LeVay (Eds.), *The Expedition 372/375 Scientists Volume 372B/375 Hikurangi Subduction Margin Coring, Logging, and Observatories. Proceedings of the International Ocean Discovery program, 372B/375*. International Ocean Discovery Program. https://doi.org/10.14379/iodp.proc.372B375.105.2019

Black, L. P., Kamo, S. L., Allen, C. M., Davis, D. W., Aleinikoff, J. N., Valley, J. W., et al. (2004). Improved 206Pb/238U microprobe geochronology by the monitoring of a trace-element-related matrix effect; SHRIMP, ID–TIMS, ELA–ICP–MS and oxygen isotope documentation for a series of zircon standards. *Chemical Geology*, *205*(1–2), 115–140. https://doi.org/10.1016/j.chemgeo.2004.01.003

Bolge, L. L., Carr, M. J., Milidakis, K. I., Lindsay, F. N., & Feigenson, M. D. (2009). Correlating geochemistry, tectonics, and volcanic volume along the Central American volcanic front. *Geochemistry, Geophysics, Geosystems*, *10*(12). https://doi.org/10.1029/2009gc002704

Booden, M. A., Smith, I. E., Mauk, J. L., & Black, P. M. (2012). Geochemical and isotopic development of the Coromandel Volcanic Zone, northern New Zealand, since 18Ma. *Journal of Volcanology and Geothermal Research*, *219–220*, 15–32. https://doi.org/10.1016/j.jvolgeores.2012.01.005

Brathwaite, R. L., & Christie, A. B. (1996). *Geology of the Waihi area, sheet T13BD & part U13, scale 1:50 000. Geological map* (Vol. 21). Institute of Geological and Nuclear Sciences.

Brenna, H., Kutterolf, S., Mills, M. J., Niemeier, T. C., & Krüger, K. (2021). Decadal disruption of the QBO by tropical volcanic supereruptions.

Briggs, R. M., Houghton, B. F., McWilliams, M., & Wilson, C. J. N. (2005). 40 Ar/39 Ar ages of silicic volcanic rocks in the Tauranga-Kaimai area, New Zealand: Dating the transition between volcanism in the Coromandel Arc and the Taupo Volcanic Zone. *New Zealand Journal of Geology and Geophysics*, *48*(3), 459–469. https://doi.org/10.1080/00288306.2005.9515126

Carey, S., & Sigurdsson, H. (2000). Grain size of Miocene volcanic ash layers from sites 998, 999, and 1000: Implications for source areas and dispersal. In R. M. Leckie, H. Sigurdsson, G. D. Acton, & G. Draper (Eds.), *Proceedings ODP, scientific results* (pp. 101–110).

Carey, S. N. (1997). Influence of convective sedimentation on the formation of widespread tephra fall layers in the deep sea. *Geology*, *25*(9), 839–842. https://doi.org/10.1130/0091-7613(1997)025<0839:iocsot>2.3.co;2

Carey, S. N. (2000). *Volcaniclastic sedimentation around island arcs*. In H. E. A. Sigurdsson (Ed.), (pp. 627–642). Academic Press. Encyclopedia of volcanoes.

Carr, M. J., Feigenson, M. D., & Bennett, E. A. (1990). Incompatible element and isotopic evidence for tectonic control of source mixing and melt extraction along the Central American Arc. *Contributions to Mineralogy and Petrology*, *105*(4), 369–380. https://doi.org/10.1007/bf00286825

Carter, L., Alloway, B., Shane, P., & Westgate, J. (2004). Deep-ocean record of major late Cenozoic rhyolitic eruptions from New Zealand. *New Zealand Journal of Geology and Geophysics*, *47*(3), 481–500. https://doi.org/10.1080/00288306.2004.9515071

Carter, L., Shane, P., Alloway, B., Hall, I. R., Harris, S. E., & Westgate, J. A. (2003). Demise of one volcanic zone and birth of another—A 12 m.y. marine record of major rhyolitic eruptions from New Zealand. *Geology*, *31*(6), 493. https://doi.org/10.1130/0091-7613(2003)031<0493:doovza>2.0.co;2

Carter, R. M., McCave, I. N., Richter, C., & Carter, L., & shipboard scientific party. (1999a). Leg 181 summary: Southwest Pacific Paleoceanography proceedings of the Ocean Drilling program, initial reports volume 181.

Carter, R. M., McCave, I. N., Richter, C., & Carter, L., & shipboard scientific party. (1999b). Site 1123: North Chatham drift—a 20-Ma record of the Pacific deep western boundary current proceedings of the Ocean Drilling program, initial reports volume 181.

Chen, C., Lee, C.-T., Tang, M., Biddle, K., & Sun, W. (2020). Lithium systematics in global arc magmas and the importance of crustal thickening for lithium enrichment. *Nature Communications*, *11*(1), 5313. https://doi.org/10.1038/s41467-020-19106-z

Cisneros de León, A., Schindlbeck-Belo, J. C., Kutterolf, S., Danišík, M., Schmitt, A. K., Freundt, A., et al. (2021). A history of violence: Magma incubation, timing and tephra distribution of the Los Chocoyos supereruption (Atitlán Caldera, Guatemala). *Journal of Quaternary Science*, *36*(2), 169–179. https://doi.org/10.1002/jqs.3265

Crundwell, M. P., & Woodhouse, A. (2022a). Biostratigraphically constrained chronologies for Quaternary sequences from the Hikurangi margin of north-eastern Zealandia. *New Zealand Journal of Geology and Geophysics*, 1–21. https://doi.org/10.1080/00288306.2022.2101481

Crundwell, M. P., & Woodhouse, A. (2022b). A detailed biostratigraphic framework for 0–1.2 Ma Quaternary sediments of north-eastern Zealandia. *New Zealand Journal of Geology and Geophysics*, 1–14. https://doi.org/10.1080/00288306.2022.2054828

Dunbar, N. W., Iverson, N. A., van Eaton, A. R., Sigl, M., Alloway, B. V., Kurbatov, A. V., et al. (2017). New Zealand supereruption provides time marker for the Last Glacial Maximum in Antarctica. *Scientific Reports*, *7*(1), 12238. https://doi.org/10.1038/s41598-017-11758-0

Elliott, T. (2003). *Tracers of the slab* (pp. 23–46). Geophysics Monograph - American Geophysical Union.

Freundt, A., Schindlbeck-Belo, J. C., Kutterolf, S., & Hopkins, J. L. (2022). *Tephra layers in the marine environment: A review of properties and emplacement processes*. Geological Society, London, Special Publications 520.

Froggatt, P. C. (1983). Toward a comprehensive upper quaternary tephra and ignimbrite stratigraphy in New Zealand using electron microprobe analysis of glass shards. *Quaternary Research*, *19*(2), 188–200. https://doi.org/10.1016/0033-5894(83)90004-2

Gardner, J. V., Nelson, C. S., & Baker, P. A. (1986). Distribution and character of pale green laminae in sediment from Lord Howe Rise: A probable late Neogene and quaternary Tephrostratigraphic record. In J. P. Kennett & C. C.von der Borch (Eds.), *Initial reports of the deep sea drilling project, 90* (Vol. 90). U.S. Government Printing Office.

Grant, G. R., Sefton, J. P., Patterson, M. O., Naish, T. R., Dunbazr, G. B., Hayward, B. W., et al. (2018). Mid-to late Pliocene (3.3–2.6 Ma) global sea-level fluctuations recorded on a continental shelf transect, Whanganui Basin, New Zealand. *Quaternary Science Reviews*, *201*, 241–260. https://doi.org/10.1016/j.quascirev.2018.09.044

Günther, D., Jackson, S. E., & Longerich, H. P. (1999). Laser ablation and arc/spark solid sample introduction into inductively coupled plasma mass spectrometers. *Spectrochimica Acta Part B: Atomic Spectroscopy*, *54*(3–4), 381–409. https://doi.org/10.1016/s0584-8547(99)00011-7

Hall, I. R., McCave, I. N., Shackleton, N. J., Weedon, G. P., & Harris, S. E. (2001). Intensified deep Pacific inflow and ventilation in Pleistocene glacial times. *Nature*, *412*(6849), 809–812. https://doi.org/10.1038/35090552

Harris, S. E. (2002). Data report: Late Pliocene–Pleistocene carbon and oxygen stable data report: Late Pliocene-Pleistocene carbon and oxygen stable isotopes from benthic foraminifers at Ocean Drilling Program Site 1123 in the Southwest Pacific. In C. Richter (Ed.), *Proceedings of the Ocean Drilling Program, Scientific Results* (Vol. 181, pp. 1–20).

Hayward, B. W., Black, P. M., Smith, I. E. M., Ballance, P. F., Itaya, T., Doi, M., et al. (2001). K-Ar ages of early Miocene arc-type volcanoes in northern New Zealand. *New Zealand Journal of Geology and Geophysics*, *44*(2), 285–311. https://doi.org/10.1080/00288306.2001.9514939

Herzer, R. H. (1995). Seismic stratigraphy of a buried volcanic arc, Northland, New Zealand and implications for Neogene subduction. *Marine and Petroleum Geology*, *12*(5), 511–531. https://doi.org/10.1016/0264-8172(95)91506-k

Hopkins, J. L., Bidmead, J. E., Lowe, D. J., Wysoczanski, R. J., Pillans, B. J., Ashworth, L., et al. (2021). TephraNZ: A major- and trace-element reference dataset for glass-shard analyses from prominent quaternary rhyolitic tephras in New Zealand and implications for correlation. *Geochronology*, *3*(2), 465–504. https://doi.org/10.5194/gchron-3-465-2021

Hopkins, J. L., Lowe, D. J., & Horrocks, J. L. (2021). Tephrochronology in Aotearoa New Zealand. *New Zealand Journal of Geology and Geophysics*, *64*(2–3), 153–200. https://doi.org/10.1080/00288306.2021.1908368

Hopkins, J. L., & Seward, D. (2019). Towards robust tephra correlations in early and pre-quaternary sediments: A case study from North Island, New Zealand. *Quaternary Geochronology*, *50*, 91–108. https://doi.org/10.1016/j.quageo.2018.12.001

Houghton, B. F., Wilson, C. J. N., McWilliams, M. O., Lanphere, M. A., Weaver, S. D., Briggs, R. M., & Pringle, M. S. (1995). Chronology and dynamics of a large silicic magmatic system: Central Taupo Volcanic Zone, New Zealand. *Geology*, *23*(1), 13. https://doi.org/10.1130/0091-7613(1995)023<0013:cadoal>2.3.co;2

Hunt, J. B., & Hill, P. G. (2001). Tephrological implications of beam size sample-size effects in electron microprobe analysis of glass shards. *Journal of Quaternary Science*, *16*(2), 105–117. https://doi.org/10.1002/jqs.571

Jarosewich, E. (2002). Smithsonian microbeam standards. *Journal of Research National. Institute of Standards and Technology*, *107*(6), 681–685. https://doi.org/10.6028/jres.107.054

Jarosewich, E., Nelen, J. A., & Norberg, J. A. (1980). Reference samples for electron microprobe analysis. *Geostandards and Geoanalytical Research*, *4*(1), 43–47. https://doi.org/10.1111/j.1751-908x.1980.tb00273.x

Jochum, K. P., Willbold, M., Raczek, I., Stoll, B., & Herwig, K. (2005). Chemical characterisation of the USGS reference GlassesGSA-1G, GSC-1G, GSD-1G, GSE-1G, BCR-2G, BHVO-2Gand BIR-1G using EPMA, ID-TIMS, ID-ICP-MS and LA-ICP-MS. *Geostandards and Geoanalytical Research*, *29*(3), 285–302. https://doi.org/10.1111/j.1751-908x.2005.tb00901.x

Julian, H. A. (2016). *Volcanology of the Owharoa and Waikino ignimbrites, Waihi, Coromandel Volcanic Zone. MSc thesis*. University of Waikato.

Jutzeler, M., Manga, M., White, J. D. L., Talling, P. J., Proussevitch, A. A., Watt, S. F. L., et al. (2017). Submarine deposits from pumiceous pyroclastic density currents traveling over water: An outstanding example from offshore Montserrat (IODP 340). *GSA Bulletin*, *129*(3–4), 392–414. https://doi.org/10.1130/b31448.1

Jutzeler, M., White, J., Talling, P. J., McCanta, M., Morgan, S., Le Friant, A., & Ishizuka, O. (2014). Coring disturbances in IODP piston cores with implications for offshore record of volcanic events and the Missoula megafloods. *Geochemistry, Geophysics, Geosystems*, *15*(9), 3572–3590. https://doi.org/10.1002/2014gc005447

Keller, J., Ryan, W., Ninkovich, D., & Altherr, R. (1978). Explosive volcanic activity in the Mediterranean over the past 200,000 yr as recorded in deep-sea sediments. *The Geological Society of America Bulletin*, *89*(4), 591. https://doi.org/10.1130/0016-7606(1978)89<591:evaitm>2.0.co;2

King, P. R. (2000). Tectonic reconstructions of New Zealand: 40 Ma to the present. *New Zealand Journal of Geology and Geophysics*, *43*(4), 611–638. https://doi.org/10.1080/00288306.2000.9514913

Kutterolf, S., Freundt, A., & Burkert, C. (2011). Eruptive history and magmatic evolution of the 1.9 kyr Plinian dacitic Chiltepe Tephra from Apoyeque volcano in west-central Nicaragua. *Bulletin of Volcanology*, *73*(7), 811–831. https://doi.org/10.1007/s00445-011-0457-0

Kutterolf, S., Freundt, A., Hansteen, T. H., Dettbarn, R., Hampel, F., Sievers, C., et al. (2021a). The medial offshore record of explosive volcanism along the Central to Eastern Aegean Volcanic Arc: 1. Tephrostratigraphic Correlations. *Geochemistry, Geophysics, Geosystems*, *22*(12). https://doi.org/10.1029/2021gc010010

Kutterolf, S., Freundt, A., Hansteen, T. H., Dettbarn, R., Hampel, F., Sievers, C., et al. (2021b). The medial offshore record of explosive volcanism along the Central to Eastern Aegean Volcanic Arc: 2. Tephra ages and volumes, eruption magnitudes and marine sedimentation rate variations. *Geochemistry, Geophysics, Geosystems*, *22*(12). https://doi.org/10.1029/2021gc010011

Kutterolf, S., Freundt, A., & Peréz, W. (2008). Pacific offshore record of Plinian Arc volcanism in Central America: 2. Tephra volumes and erupted masses. *Geochemistry, Geophysics, Geosystems*, *9*. https://doi.org/10.1029/2007gc001791

Kutterolf, S., Freundt, A., Peréz, W., Mörz, T., Schacht, U., Wehrmann, H., & Schmincke, H.-U. (2008). Pacific offshore record of Plinian Arc volcanism in Central America: 1. Along-Arc correlations. *Geochemistry, Geophysics, Geosystems*, *9*(2). https://doi.org/10.1029/2007gc001631

Kutterolf, S., Jegen, M., Mitrovica, J. X., Kwasnitschka, T., Freundt, A., & Huybers, P. J. (2013). A detection of Milankovitch frequencies in global volcanic activity. *Geology*, *41*(2), 227–230. https://doi.org/10.1130/g33419.1

Kutterolf, S., Schindlbeck, J. C., Jegen, M., Freundt, A., & Straub, S. M. (2019). Milankovitch frequencies in tephra records at volcanic arcs: The relation of kyr-scale cyclic variations in volcanism to global climate changes. *Quaternary Science Reviews*. https://doi.org/10.1016/j.quascirev.2018.11.004

Ledbetter, M. T. (1985). Tephrochronology of marine tephra adjacent to Central America. *The Geological Society of America Bulletin*, *96*(1), 77. https://doi.org/10.1130/0016-7606(1985)96<77:tomtat>2.0.co;2

Le Maitre, R. W., Streckeisen, A., Zanettin, B., Le Bas, M. J., Bonin, B., Bateman, P., et al. (2002). Igneous rocks: A classification and glossary of terms: Recommendations of the International Union of Geological Sciences subcommission of the systematics of igneous rocks.

Lowe, D. J. (1990). Tephra studies in New Zealand: An historical review. *Journal of the Royal Society of New Zealand*, *20*(1), 119–150. https://doi.org/10.1080/03036758.1990.10426736

Lowe, D. J. (2011). Tephrochronology and its application: A review. *Quaternary Geochronology*, *6*(2), 107–153. https://doi.org/10.1016/j.quageo.2010.08.003

Manville, V., & Wilson, C. J. N. (2004). Vertical density currents: A review of their potential role in the deposition and interpretation of deep-sea ash layers. *Journal of the Geological Society of London*, *161*(6), 947–958. https://doi.org/10.1144/0016-764903-067

Münker, C. (2000). The isotope and trace element budget of the Cambrian Devil River Arc System, New Zealand: Identification of four source components. *Journal of Petrology*, *41/6*(6), 759–788. https://doi.org/10.1093/petrology/41.6.759

Naish, T., Kamp, P. J., Alloway, B. V., Pillans, B., Wilson, G. S., & Westgate, J. A. (1996). Integrated tephrochronology and magnetostratigraphy for cyclothemic marine strata, Wanganui Basin: Implications for the Pliocene-Pleistocene boundary in New Zealand. *Quaternary International*, *34–36*, 29–48. https://doi.org/10.1016/1040-6182(95)00067-4

Nelson, C. S., Froggatt, P. C., & Gosson, G. J. (1986). Nature, chemistry, and origin of Late Cenozoic megascopic tephras in Leg 90 cores from the Southwest Pacific. In J. P. Kennett & C. C.von der Borch (Eds.), *Initial reports of the deep Sea Drilling project, 90* (Vol. 90). U.S. Government Printing Office.

Norman, M. D., Pearson, N. J., Sharma, A., & Griffin, W. L. (1996). Quantitative analysis of trace elements in geological materials by laser ablation ICPMS: Instrumental operating conditions and calibration values of NIST glasses. *Geostandards and Geoanalytical Research*, *20*(2), 247–261. https://doi.org/10.1111/j.1751-908x.1996.tb00186.x

Pank, K., Kutterolf, S., Hopkins, J. L., Wang, K.-L., & Lee, H.-Y. (2023). Data report: Marine tephra compositions in proximal and distal drill cores, IODP expeditions 375, 372, and 329, ODP Leg 181, and DSDP Leg 90, offshore New Zealand, southwest Pacific. In *Proceedings of the International Ocean Discovery program volume 372B/375 - Hikurangi subduction margin coring, logging, and observatories*. https://doi.org/10.14379/iodp.proc.372B375.210.2023

Pearce, N., Westgate, J. A., Gualda, G., Gatti, E., & Muhammad, R. F. (2020). Tephra glass chemistry provides storage and discharge details of five magma reservoirs which fed the 75ka youngest Toba Tuff eruption, Northern Sumatra. *Journal of Quaternary Science*, *35*(1–2), 256–271. https://doi.org/10.1002/jqs.3149

Peccerillo, A., & Taylor, S. R. (1976). Geochemistry of Eocene calc-alkaline volcanic rocks from the Kastamonu area, Northern Turkey. *Contributions to Mineralogy and Petrology*, *58*(1), 63–81. https://doi.org/10.1007/bf00384745

Pfänder, J. A., Jung, S., Münker, C., Stracke, A., & Mezher, K. (2012). A possible high Nb/Ta reservoir in the continental lithospheric mantle and consequences on the global Nb budget – Evidence from continental basalts from Central Germany. *Geochimica et Cosmochimica Acta*, *77*, 232–251. https://doi.org/10.1016/j.gca.2011.11.017

Pillans, B., Alloway, B., Naish, T., Westgate, J., Abbott, S., & Palmer, A. (2005). Silicic tephras in Pleistocene shallow-marine sediments of Wanganui Basin, New Zealand. *Journal of the Royal Society of New Zealand*, *35*(1–2), 43–90. https://doi.org/10.1080/03014223.2005.9517777

Pittari, A., Prentice, M. L., McLeod, O. E., Yousef Zadeh, E., Kamp, P. J. J., Danišík, M., & Vincent, K. A. (2021). Inception of the modern North Island (New Zealand) volcanic setting: Spatio-temporal patterns of volcanism between 3.0 and 0.9 Ma. *New Zealand Journal of Geology and Geophysics*, *64*, 250–272. https://doi.org/10.1080/00288306.2021.1915343

Plank, T. (2014). The chemical composition of subducting sediments. *Treatise Geochem*, 607–629.

Pole, M. (2003). New Zealand climate in the Neogene and implications for global atmospheric circulation. *Palaeogeography, Palaeoclimatology, Palaeoecology*, *193*(2), 269–284. https://doi.org/10.1016/s0031-0182(03)00232-3

Pouderoux, H., Proust, J.-N., Lamarche, G., Orpin, A., & Neil, H. (2012). Postglacial (after 18ka) deep-sea sedimentation along the Hikurangi subduction margin (New Zealand): Characterisation, timing and origin of turbidites. *Marine Geology*, *295–298*, 51–76. https://doi.org/10.1016/j.margeo.2011.11.002

Rea, D. K., & Bloomstine, M. K. (1986). Neogene history of the south Pacific tradewinds: Evidence for hemispherical asymmetry of atmospheric circulation. *Palaeogeography, Palaeoclimatology, Palaeoecology*, *55*(1), 55–64. https://doi.org/10.1016/0031-0182(86)90137-9

Ryan, W. B. F., Carbotte, S. M., Coplan, J. O., O'Hara, S., Melkonian, A., Arko, R., et al. (2009). Global multi-resolution topography synthesis. *Geochemistry, Geophysics, Geosystems*, *10*(3). https://doi.org/10.1029/2008gc002332

Schindlbeck, J. C., Jegen, M., Freundt, A., Kutterolf, S., Straub, S. M., Mleneck-Vautravers, M. J., & McManus, J. F. (2018). 100-kyr cyclicity in volcanic ash emplacement: Evidence from a 1.1Myr tephra record from the NE Pacific. *Scientific Reports*, *8*(1), 4440. https://doi.org/10.1038/s41598-018-22595-0

Schindlbeck, J. C., Kutterolf, S., Freundt, A., Alvarado, G. E., Wang, K.-L., Straub, S. M., et al. (2016b). Late Cenozoic tephrostratigraphy offshore the southern Central American Volcanic Arc: 1. Tephra ages and provenance. *Geochemistry, Geophysics, Geosystems*. https://doi.org/10.1002/2016GC006503

Schindlbeck, J. C., Kutterolf, S., Freundt, A., Eisele, S., Wang, K.-L., & Frische, M. (2018b). Miocene to Holocene Marine Tephrostratigraphy Offshore Northern Central America and Southern Mexico: Pulsed activity of known volcanic complexes. *Geochemistry, Geophysics, Geosystems*, *19*(11), 4143–4173. https://doi.org/10.1029/2018gc007832

Schindlbeck, J. C., Kutterolf, S., Freundt, A., Straub, S. M., Vannucchi, P., & Alvarado, G. E. (2016). Late Cenozoic tephrostratigraphy offshore the southern Central American Volcanic Arc: 2. Implications for magma production rates and subduction erosion. *Geochemistry, Geophysics, Geosystems*. https://doi.org/10.1002/2016GC006504.

Sefton, J. P. (2015). *An assessment of the influence of orbital forcing on Late Pliocene global sea-level using a shallow-marine sedimentary record from the Wanganui Basin, New Zealand. MSc thesis*. University of Wellington.

Shane, P. (2000). Tephrochronology: A New Zealand case study. *Earth-Science Reviews*, *49*(1–4), 223–259. https://doi.org/10.1016/s0012-8252(99)00058-6

Shane, P., Black, T., Eggins, S., & Westgate, J. (1998). Late Miocene marine tephra beds: Recorders of rhyolitic volcanism in North Island, New Zealand. *New Zealand Journal of Geology and Geophysics*, *41*(2), 165–178. https://doi.org/10.1080/00288306.1998.9514801

Skinner, D. (1986). Neogene volcanism of the Hauraki Volcanic Region. *Bulletin - Royal Society of New Zealand*, 21–47.

Skinner, D. N. B. (1976). *Sheet N40 and pts N35, N36, N39-Northern Coromandel. Geological map of New Zealand 1:63 360*. Department of Scientific and Industrial Research.

Skinner, D. N. B. (1993). *The geology of Coromandel Harbour (sheets S11 east: T11 west). Geological map of New Zealand 1:50 000*. Institute of Geological and Nuclear Sciences Ltd map 4. Lower Hutt.

Smith, I., Ruddock, R. S., & Day, R. A. (1989). Miocene arc-type volcanic/plutonic complexes of the Northland Peninsula, New Zealand. *Bulletin - Royal Society of New Zealand*, 205–213.

Smith, V. C., Isaia, R., Engwell, S. L., & Albert, P. G. (2016). Tephra dispersal during the Campanian Ignimbrite (Italy) eruption: Implications for ultra-distal ash transport during the large caldera-forming eruption. *Bulletin of Volcanology*, *78*(6), 45. https://doi.org/10.1007/s00445-016-1037-0

Stacey, J. S., & Kramers, J. D. (1975). Approximation of terrestrial lead isotope evolution by a two-stage model. *Earth and Planetary Science Letters*, *26*(2), 207–221. https://doi.org/10.1016/0012-821x(75)90088-6

Stevens, M. T. (2010). *Miocene and Pliocene silicic Coromandel Volcanic Zone tephras from ODP site 1124-C: Petrogenetic applications and temporal evolution: Master thesis submitted to School of Geography, Environment and Earth Sciences*. Victoria University of Wellington.

Stipp, J. J. (1968). *The geochronology and petrogenesis of the Cenozoic Volcanics of North Island, New Zealand: PhD thesis submitted in the Australian*. National University.

Strogen, D. P., Seebeck, H., Hines, B. R., Bland, K. J., & Crampton, J. S. (2022). Paleogeographic evolution of Zealandia: Mid-Cretaceous to present. *New Zealand Journal of Geology and Geophysics*, 1–30. https://doi.org/10.1080/00288306.2022.2115520

van Achterberg, E., Ryan, C. G., Jackson, S. E., & Griffin, W. (2001). LA-ICP-MS. In P. J. Sylvester (Ed.), *The earth sciences - appendix 3, data reduction software for LA-ICP-MS, Short course volume 29*. St.John's, Mineralogical Association of Canada. (pp. 239–243).

Waight, T., Troll, V. R., Gamble, J. A., Price, R. C., & Chadwick, J. P. (2017). Hf isotope evidence for variable slab input and crustal addition in basalts and andesites of the Taupo Volcanic Zone, New Zealand. *Lithos*, *284–285*, 222–236. https://doi.org/10.1016/j.lithos.2017.04.009

Walker, J., Mickelson, E., Thomas, R. B., Patino, L. C., Cameron, B., Carr, M. J., et al. (2007). U-series disequilibria in Guatemalan lavas, crustal contamination, and implications for magma Genesis along the Central American subduction zone. *Journal of Geophysical Research*, *112*(B6), B06205. https://doi.org/10.1029/2006jb004589

Wallace, L. M., Saffer, D. M., Barnes, P. M., Pecher, I. A., Petronotis, K. E., LeVay, L. J., et al. (2019). Expedition 372B/375 methods. In L. M. Wallace, D. M. Saffer, P. M. Barnes, I. A. Pecher, K. E. Petronotis, & L. J. LeVay (Eds.). *The Expedition on 372/375 Scientists Hikurangi Subduction Margin Coring, Logging, and Observatories. Proceedings of the International Ocean Discovery Program, 372B/375*. International Ocean Discovery Program.

Wiedenbeck, M., Allé, P., Corfu, F., Griffin, W. L., Meier, M., Oberli, F., et al. (1995). Three natural zircon standards for U–Th–Pb, Lu–Hf, trace element and REE analyses. *Geostandards and Geoanalytical Research*, *19*, 1–23. https://doi.org/10.1111/j.1751-908x.1995.tb00147.x

Wilson, C. J., & Rowland, J. V. (2016). The volcanic, magmatic and tectonic setting of the Taupo Volcanic Zone, New Zealand, reviewed from a geothermal perspective. *Geothermics*, *59*, 168–187. https://doi.org/10.1016/j.geothermics.2015.06.013

Wilson, C. J. N., Houghton, B. F., McWilliams, M. O., Lanphere, M. A., Weaver, S. D., & Briggs, R. M. (1995). Volcanic and structural evolution of Taupo Volcanic Zone, New Zealand: A review. *Journal of Volcanology and Geothermal Research*, *68*(1–3), 1–28. https://doi.org/10.1016/0377-0273(95)00006-g

Woodhouse, A., Barnes, P. M., Shorrock, A., Strachan, L. J., Crundwell, M., Bostock, H. C., et al. (2022). Trench floor depositional response to glacio-eustatic changes over the last 45 ka, northern Hikurangi subduction margin, New Zealand. *New Zealand Journal of Geology and Geophysics*, 1–24. https://doi.org/10.1080/00288306.2022.2099432

Zamboni, D. E., Gazel, J. G., Ryan, C., Cannatelli, F., Lucchi, Z. D., Atlas, J., et al. (2016). Contrasting sediment melt and fluid signatures for magma components in the Aeolian Arc: Implications for numerical modeling of subduction systems. *Geochemistry, Geophysics, Geosystems*, *17*(6), 2034–2053. https://doi.org/10.1002/2016gc006301

Zirakparvar, N. A. (2016). Constraints on Lu-Hf and Nb-Ta systematics in globally subducted oceanic crust from a survey of orogenic eclogites and amphibolites. *Geochemistry, Geophysics, Geosystems*, *17*(4), 1540–1557. https://doi.org/10.1002/2016gc006377